Integrated Aerodynamic/Dynamic/Structural Optimization of Helicopter Rotor Blades Using Multilevel Decomposition

Joanne L. Walsh and Katherine C. Young
Langley Research Center • Hampton, Virginia

Jocelyn I. Pritchard
Vehicle Structures Directorate
U.S. Army Research Laboratory
Langley Research Center • Hampton, Virginia

Howard M. Adelman
Langley Research Center • Hampton, Virginia

Wayne R. Mantay
Joint Research Program Office
Aeroflightdynamics Directorate
U.S. Army Aviation and Troop Command
Langley Research Center • Hampton, Virginia

January 1995

This publication is available from the following sources:

Summary

This paper describes an integrated aerodynamic/dynamic/structural (IADS) optimization procedure for helicopter rotor blades. The procedure combines performance, dynamics, and structural analyses with a general-purpose optimizer using multilevel decomposition techniques. At the upper level, the structure is defined in terms of global quantities (stiffnesses, masses, and average strains). At the lower level, the structure is defined in terms of local quantities (detailed dimensions of the blade structure and stresses).

The upper level objective function is a linear combination of performance and dynamic measures. Upper level design variables include pretwist, point of taper initiation, taper ratio, root chord, blade stiffnesses, tuning masses, and tuning mass locations. Upper level constraints consist of limits on power required in hover, forward flight, and maneuver; airfoil drag; minimum tip chord; trim; blade natural frequencies; autorotational inertia; blade weight; and average strains.

The lower level sizes the internal blade structure at several radial locations along the blade. The lower level optimization assures that a structure can be sized to provide the stiffnesses required by the upper level and also assures the structural integrity of the blade. The lower level design variables are the box beam wall thicknesses and several lumped areas that are analogous to longitudinal stringers in a wing box cross section. The lower level objective function is a measure of the difference between the upper level stiffnesses and the stiffnesses computed from the wall thicknesses and lumped areas. Lower level constraints are on the Von Mises stress at the box corners for multiple-load cases generated by several flight conditions, limits on wall thicknesses for thin-wall theory, and other dimensional considerations.

The IADS procedure provides an optimization technique that is compatible with industrial design practices in which the aerodynamic and dynamic designs are performed at a global level and the structural design is carried out at a detailed level with considerable dialogue and compromise among the aerodynamic, dynamic, and structural groups. The IADS procedure is demonstrated for several cases.

Introduction

Over the last decade, optimization techniques have been studied for application to the rotor blade design process. In reference 1, Miura presents a survey on the application of numerical optimization methods to helicopter design problems including rotor blade design. Most optimization procedures have dealt with a single discipline such as aerodynamics (refs. 2–4), structures (ref. 5), or dynamics (refs. 2 and 6–9). However, the rotor blade design process is multidisciplinary involving couplings and interactions between several disciplines such as aerodynamics, dynamics, structures, and acoustics. These couplings and interactions can be exploited by the optimization procedure if all the disciplines are accounted for simultaneously rather than sequentially. For instance, in a review (ref. 10) on the impact of structural optimization on vibration reduction, Friedmann emphasizes the need to include the multidisciplinary couplings between aerodynamics, dynamics, and structures even when optimizing only for minimum vibration.

Techniques and strategies for merging disciplines to obtain integrated rotorcraft optimization procedures are developing. In references 11 and 12, a plan is described for integrating the disciplines of aerodynamics, dynamics, structures, and acoustics. As part of that plan, aerodynamics and dynamics have been incorporated systematically into performance (refs. 3 and 4) and airload/dynamic (ref. 13) optimization procedures resulting in an integrated aerodynamic/dynamic optimization procedure (ref. 14). Reference 15 summarizes recent accomplishments based on that plan.

Other multidisciplinary rotor blade optimization work is described in references 16–19. References 16 and 17 describe the formulation of a multidisciplinary approach to rotor blade design for improved performance and reduced fuselage vibrations. Reference 18 describes a staged optimization procedure for a rotor for combined aerodynamics, dynamics, and structures. Reference 19 describes a multidisciplinary optimization procedure to design high-speed prop rotors.

What is lacking in previous multidisciplinary rotor blade optimization procedures is an efficient method to integrate structures or structural properties. Usually, structures or structural properties are included in one of two ways—either as local design variables (indirectly affecting the response of the blade) or as global design variables (directly affecting the response of the blade). When local design variables are used, the detail dimensions of a structural member at one or more radial locations along the blade are used to generate structural properties. When global design variables are used, structural properties are the design variables. Both types of design variables have limitations. Using local design variables (e.g., refs. 6, 7, 18, and 19), such as wall

thicknesses of the structural member, can lead to a large number of design variables that can be computationally expensive. Also, this choice of design variables is at odds with the traditional design practice in which chord, stiffness, and mass distributions along the blade are determined and then a structure is designed that matches these distributions. Using global design variables (e.g., refs. 2, 9, 13, 14, 16, and 17), such as stiffness and mass properties, in optimization also has disadvantages. When flapwise bending stiffness, chordwise bending stiffness, torsional stiffness, and extensional stiffness distributions are used as design variables, they are treated as independent quantities. In reality, these stiffnesses are not independent, and no guarantee can be given that a set of wall thicknesses can be found that will simultaneously give these stiffnesses.

This paper presents the methodology for incorporating aerodynamics, dynamics, and structures in an integrated optimization procedure using both local and global design variables. Multilevel decomposition techniques based on reference 20 are used to add structural design variables and constraints to an existing aerodynamic/dynamic optimization procedure (ref. 14). The product is an integrated aerodynamic/dynamic/structural (IADS) optimization procedure. The multilevel formulation used in this paper was presented first in reference 15. Another preliminary study of multilevel techniques applied to rotor blade design is described in reference 21.

The multilevel decomposition approach has been successfully applied to multidisciplinary problems (e.g., refs. 22–24). As originally proposed in reference 25, the coordination procedure consisted of an optimum sensitivity analysis (ref. 26) and a set of equality constraints that relate the detailed (local) design variables of one subsystem to the global design variables on the level above. However, as pointed out in reference 27, these equality constraints have caused difficulties in implementing multilevel decomposition procedures. The IADS procedure is based on the multilevel decomposition approach of reference 20 which eliminates the equality constraints in the coordination procedure, thus allowing the use of the optimum sensitivity derivative found in reference 28 that is less computationally costly. However in the IADS procedure, the set of lower level constraints is replaced by an envelope function known as the Kreisselmeir-Steinhauser function (KS function, ref. 29) which further reduces the computational cost.

First, the general multilevel decomposition strategy with two levels will be discussed. (Note that the systems with more levels are discussed in refs. 20, 22, and 25.) Next, the general strategy will be related to rotor blade design. Then, the IADS development including flowcharts of the upper and lower levels and the optimization procedure will be explained. Results will be presented for several cases that demonstrate the strengths of the IADS procedure.

Symbols and Abbreviations

A	area, ft^2
AI	autorotational inertia, $\sum_{j=1}^{ns} W_j r_j^2$, lbm-ft^2
a_i	ith lumped area, ft^2
b	box width, ft
C_D	rotor coefficient of drag
C_L	rotor coefficient of lift
CF	centrifugal force, lb
c_d	airfoil section drag coefficient
$c_{d,all}$	maximum allowable section drag coefficient
$c_{d,\max}^{\Psi}$	largest section drag coefficient at azimuth angle Ψ
c_l	airfoil section lift coefficient
c_r	root chord, ft
c_t	tip chord, ft
DV_p	pth upper level design variable
E	Young's modulus of elasticity, lb/ft^2
EA	extensional stiffness, lb
EI_{xx}	chordwise bending stiffness, lb-ft^2
EI_{zz}	flapwise bending stiffness, lb-ft^2
F	lower level objective function
$f_{b,i}$	ith bending frequency, per rev
f_k	kth frequency, per rev
$f_{k,l}$	lower bound on kth frequency, per rev
$f_{k,u}$	upper bound on kth frequency, per rev
$f_{t,i}$	ith torsional frequency, per rev
Δf	increment used in frequency window, per rev
G	torsional modulus of elasticity, lb/ft^2
GJ	torsional stiffness, lb-ft^2

$g_{c,i}$	ith lower level constraint function
g_i	ith upper level constraint function
g_{max}	maximum lower level constraint function, $\max\{g_{c,i}\}$
h	box height, ft
ITER	number of trim iterations
I_{xx}	chordwise moment of inertia, ft^4
I_{zz}	flapwise moment of inertia, ft^4
J	polar moment of inertia, ft^4
KS	Kreisselmeir-Steinhauser function
k_i	ith weighting factor in objective function
l_f	factor of safety
MRA	total number of aerodynamic segments
m_i	ith segment tuning mass, slug/ft
N	number of blades
NDV	number of upper level design variables
n	integer
nc	number of constraint components in lower level
nP	frequency at n times the rotational speed of the blade
ns	number of structural segments
OBJ	upper level objective function
P	main rotor power, hp
R	blade radius from center of rotation, ft
r	distance along blade from center of rotation, ft
r_j	distance from center of rotation to center of jth segment, ft
$S_{N,ff}$	N/rev rotating vertical hub shear in forward flight, lbf
$S_{N,ref}$	reference value of N/rev rotating vertical hub shear in forward flight, lbf
$S_{4,ff}$	4/rev rotating vertical hub shear in forward flight, lbf

$S_{4,ref}$	reference value of 4/rev rotating vertical hub shear in forward flight, lbf
t_k	kth wall thickness, ft
t_{max}	nondimensional location of maximum airfoil thickness
$V(\sigma,\tau)$	Von Mises stress, lb/ft^2
v_i	ith lower level design variable
W	total blade weight, lbm
W_j	total weight of jth structural segment, lbm
x_l	nondimensional distance from airfoil leading edge to left of wing box
x_r	nondimensional distance from airfoil trailing edge to right of wing box
y_i	location of ith tuning mass
y_{tr}	point of taper initiation
z_l	nondimensional lower airfoil coordinate
z_u	nondimensional upper airfoil coordinate
ε	coordination parameter
ε_a	allowable average strain
ε_y	average strain
θ_{tw}	maximum pretwist, deg
λ	Lagrange multiplier
ρ	pull-down factor
σ	bending stress, lb/ft^2
σ_a	allowable stress, lb/ft^2
τ	shear stress, lb/ft^2
Ψ	azimuth angle, zero over tail, deg
Ω	rotor speed, rpm

Subscripts:

a	available
ff	forward flight
h	hover
m	maneuver
max	maximum
min	minimum
o	optimum
ref	reference

Superscripts:

i ith component

L lower level

T transpose

U upper level

A bar over a symbol indicates a nondimensional quantity, and an asterisk (*) used as a superscript indicates an upper level design variable.

Multilevel Optimization Strategy

With a multilevel decomposition approach (refs. 20, 22, and 25), a large complex optimization problem is broken into a hierarchy of smaller optimization subproblems. This hierarchy can be thought of as levels of increasing detail. At the upper level, the subproblem is formulated in terms of global quantities that describe the overall behavior of the entire system. On the lower level, the subproblems are stated in terms of local quantities and local constraints that have only a small impact on the entire system. Each of these subproblems use local design variables to reduce the violation of constraints that are unique to that subproblem. The coupling between the upper level subproblem and the lower level subproblems is preserved through a coordination procedure such as that described in references 20 or 25. This coupling represents a dialogue between the levels that, upon convergence, establishes compatibility between the two levels.

Figure 1 illustrates a generic two-level optimization procedure. Note that the analysis proceeds from the upper level to the lower level while the optimization proceeds from the lower level to the upper level. First, the upper level analysis initializes all the global quantities and responses and then provides information to each lower level subproblem. Next, individual lower level optimizations are performed that reduce local constraints as much as possible and that provide information to the coordination procedure. Finally, the upper level optimization occurs. The preceding description defines 1 cycle. This entire process is repeated for several cycles. Convergence occurs when all the constraints (both upper level and lower level) are satisfied and the upper level objective function is minimized.

The rotor blade optimization problem can be decomposed into one subproblem affecting the global response of the blade and three subproblems affecting portions of the blade. Quantities such as power required, blade trim, autorotational inertia, natural frequencies, total blade weight, and average strain describe the global response of the blade. The entire blade must be analyzed to obtain these response quantities. Quantities such as stresses are detailed response quantities since only a portion of the blade must be considered to obtain these response quantities. Therefore, a two-level decomposed rotor blade optimization problem can be defined as shown in figure 2. The upper level optimizes the blade by changing global quantities such as blade planform, twist, and distributions of mass and stiffness. The upper level chord, mass, and stiffness distributions are treated as independent quantities. The reconciliation between these distributions is done on the lower level, which consists of several independent subproblems at stations along the blade radius. These subproblems optimize detailed cross-sectional dimensions to satisfy stress constraints and to reconcile the upper level independent mass, chord, and stiffness distributions with the lower level calculated mass and stiffness distributions. This reconciliation is improved further by a set of upper level coordination constraints. (See appendix A.) First, the upper level analysis and optimization will be described, then the lower level analysis and optimization, and last the overall IADS system.

Upper Level Analysis and Optimization

The purpose of the upper level analysis is to evaluate the overall rotor blade design on the basis of performance, dynamic, and global structural measures. (For a description of the rotor blade design philosophy, see refs. 3, 4, 11, 12, 14, and 15.) The upper level analysis is similar to the integrated aerodynamic/dynamic analysis reported in reference 14 with the addition of extensional stiffness design variables, strain constraints, and coordination constraints. As shown in figure 3, the blade is evaluated for three flight conditions: hover, forward flight, and maneuver. The Langley-developed hover analysis program HOVT (a blade-element momentum analysis based on ref. 30) is used to predict power required in hover. The comprehensive helicopter analysis program CAMRAD/JA (ref. 31) is used to predict rotor performance (e.g., trim, airfoil drag, and power required), loads, and frequencies for forward flight and maneuver. The maneuver flight condition simulates a coordinated turn in terms of an increased load on the forward-flight lift requirement.

The rotor blade design process is defined in terms of aerodynamic performance, dynamics, and global structural requirements. Satisfactory aerodynamic performance is defined by the following four requirements. First, the power required for any flight

condition must be less than the available power. Second, airfoil section drag along the blade radius on the advancing and retreating side of the rotor disk in both forward flight and maneuver must be less than a maximum allowable value. Third, the rotor must trim at each flight condition. The rotor is trimmed to a constant lift in forward flight and a (different) constant lift in maneuver which ensures that the rotor has no loss in lift capability or maneuverability even if solidity decreases from the initial to the final design. Incorporation of a maneuver flight condition is used in place of a constraint on solidity, because low-speed maneuver determines rotor solidity (ref. 32). Fourth, the blade tip chord must be larger than a prescribed minimum value. Satisfactory dynamics is defined in terms of limits on vibrational frequencies. The blade is designed so that the natural frequencies (both bending and torsional) do not coincide with integer multiples of the rotor speed. Also, the blade must have sufficient autorotational inertia as a safety measure needed in case of engine failure. In addition to satisfying these design requirements, the blade weight must not exceed some upper limit. Satisfactory structural requirements are defined in terms of limits on the average axial strains for forward flight and maneuver flight conditions. The upper level optimization problem is formulated next in terms of design variables, objective function, and constraints.

Upper Level Design Variables

The upper level design variables are the blade planform, stiffnesses, and tuning masses. (See fig. 4.) The blade planform is defined by the point of taper initiation (y_{tr}), root chord (c_r), taper ratio (c_r/c_t), and maximum pretwist (θ_{tw}). The blade is rectangular from the root to y_{tr} and then tapers linearly to the tip. The pretwist varies linearly from the center of rotation to the tip. Global design variables include the blade chordwise, flapwise, torsional, and extensional stiffnesses (denoted by EI_{xx}, EI_{zz}, GJ, and EA, respectively) at three radial locations: blade root, point of taper initiation, and blade tip. The stiffnesses are assumed to vary linearly between these points and are treated as independent quantities. The remaining design variables are three tuning masses (denoted by m_1, m_2, and m_3) and their locations (denoted by y_1, y_2, and y_3), respectively. The total blade mass consists of the structural mass (which is assumed to be constant) plus the sum of the tuning masses. No attempt is made to reconcile the change in weight with the change in design variables because the present work is based on extending the procedure of reference 14 to include structures. However, this reconciliation is possible. (See ref. 15.)

The center of gravity and aerodynamic offsets are coincident with the blade elastic axis. The number of blades, rotor radius, rotational velocity, airfoils, and airfoil distribution are preselected and fixed.

Upper Level Objective Function

The objective function to be minimized is a combination of performance and dynamics measures and is formulated as

$$\text{OBJ} = k_1 \frac{P_h}{P_{h,\text{ref}}} + k_2 \frac{P_{ff}}{P_{ff,\text{ref}}} + k_3 \frac{P_m}{P_{m,\text{ref}}} + k_4 \frac{S_{N,ff}}{S_{N,\text{ref}}} \quad (1)$$

where P_h, P_{ff}, and P_m are the powers required in hover, forward flight, and maneuver, respectively. The symbol N is the number of blades, and $S_{N,ff}$ is the N/rev rotating vertical hub shear in forward flight. The terms k_1, k_2, k_3, and k_4 are weighting factors chosen by the user, and $P_{h,\text{ref}}, P_{ff,\text{ref}}, P_{m,\text{ref}}$, and $S_{N,\text{ref}}$ are reference values used to normalize and nondimensionalize the objective function components. The usefulness of this objective function was demonstrated in reference 14.

Upper Level Constraints

The upper level constraints are grouped into performance, dynamic, structural, and coordination constraints. This section of the paper discusses the performance, dynamic, and structural constraints. The coordination constraints are discussed later in the paper. The performance and dynamic constraints are the same as those used in reference 14. By convention, the ith constraint g_i is satisfied if it is less than or equal to zero.

Performance constraints. The performance constraints are on power required, trim, airfoil section drag, and blade tip chord. The requirement that the power required be less than the power available is given by

$$g_i = \frac{P_j}{P_a} - 1 \leq 0 \quad (2)$$

for each flight condition, where P_j is the power required for the ith flight condition and P_a is the power available.

The requirement on the airfoil section drag translates into a constraint that each airfoil section distributed along the rotor blade operate at a section drag coefficient c_d less than a specified allowable value $c_{d,\text{all}}$. (See appendix B.) This leads to 24 constraints per flight condition because the blade is analyzed in azimuth increments of $15°$ around the rotor disk. At

5

a given azimuth angle (Ψ), the constraint is formulated as

$$g_i = \frac{c_{d,\max}^{\Psi}}{c_{d,\text{all}}} - 1 \leq 0 \quad (\Psi = 15°, 30°, 45°, \ldots, 360°) \quad (3)$$

where $c_{d,\text{all}}$ is the allowable drag coefficient and $c_{d,\max}^{\Psi}$ is the largest drag coefficient at any radial station. (Note that the drag coefficients in the reverse-flow region occurring on the retreating side of the rotor disk are ignored.) In the present work, the same value for $c_{d,\text{all}}$ is used on the advancing and retreating side of the rotor disk. This simplifying assumption can easily be lifted.

The trim requirement is difficult to translate into a mathematical constraint. The trim constraints in forward flight and maneuver are implemented by using the method developed in reference 3, which expresses the constraint in terms of the number of trim iterations (ITER), the maximum number of trim iterations allowed (ITER$_{\max}$), and the pth nondimensional design variable ($\overline{\text{DV}}_p$). The heuristic trim constraint is given by

$$g_i = (\text{ITER} - \text{ITER}_{\max} + 1)\left(\sum_{p=1}^{\text{NDV}} \overline{\text{DV}}_p\right) \leq 0 \quad (4)$$

where NDV is the number of design variables. In the development of this equation in reference 3, the addition of the summation term was found to improve convergence because it allowed calculation of the change in the trim constraint with respect to the change in a single design variable.

The final performance requirement is a constraint used to ensure that the blade tip chord does not become too small. Thus,

$$g_i = 1 - \frac{c_t}{c_{t,\min}} \leq 0 \quad (5)$$

where c_t is the tip chord and $c_{t,\min}$ is the minimum tip chord allowed. This is a practical constraint used to assure validity of the airfoil tables and to address manufacturing considerations.

Dynamic constraints. The dynamic constraints are on frequencies, total blade weight, and autorotational inertia. The constraint on the kth frequency f_k (either a bending or a torsional frequency) is formulated such that the frequency is separated from integer multiples of the rotor speed by

an amount Δf. Thus, for the upper bound,

$$g_i = \frac{f_k}{f_{k,u}} - 1 \leq 0 \quad (6a)$$

and for the lower bound,

$$g_i = 1 - \frac{f_k}{f_{k,l}} \leq 0 \quad (6b)$$

where $f_{k,u}$ has a value that is Δf below $n+1$ per rev and $f_{k,l}$ has a value that is Δf above n/rev for the applicable n. For example, if Δf is 0.1/rev and f_4 is 5.6/rev, then nP would be 5/rev and $(n+1)P$ would be 6/rev. Thus, $f_{4,u}$ and $f_{4,l}$ would be 5.9/rev and 5.1/rev, respectively. Formulating the constraints in this manner allows the frequencies to change from one optimization cycle to the next cycle provided the frequencies avoid approaching integer multiples of the rotor speed. This formulation is different from the approaches used in references 13, 16, and 17 in which the frequencies are kept within prescribed windows based on the reference blade frequencies. In this work, constraints are placed on frequencies in both forward flight and maneuver because blade collective pitch and the amount of modal coupling may be different for the two flight conditions, and therefore the frequencies can be different.

The constraint that the blade weight should be less than some maximum value is formulated as

$$g_i = \frac{W}{W_{\max}} - 1 \leq 0 \quad (7)$$

where W is the total blade weight and $W_{\max}$ is the maximum allowable weight. The total blade weight is the structural mass distribution (which is constant) plus the sum of the tuning masses.

Finally, the blade must have enough autorotational inertia (AI) for safe autorotation in case of engine failure. The constraint is formulated so that the autorotational inertia of the blade is greater than some minimum value AI$_{\min}$. Thus,

$$g_i = 1 - \frac{\text{AI}}{\text{AI}_{\min}} \leq 0 \quad (8)$$

Structural constraints. The structural constraints are on the average axial strains. The structural constraints evaluated at the same radial locations that are used to define the design variables (fig. 4) are imposed on the average axial strains (ε_y) as follows:

$$g_i = \frac{\varepsilon_y}{\varepsilon_a} - 1 \leq 0 \quad (9a)$$

and

$$g_i = -1 - \frac{\varepsilon_y}{\varepsilon_a} \leq 0 \qquad (9b)$$

where ε_a is the magnitude of the allowable strain and

$$\varepsilon_y = \frac{l_f \, \text{CF}}{EA} \qquad (10)$$

where CF is the centrifugal force, EA is the extensional stiffness, and l_f is a safety factor on the loads. The strain constraints are calculated using loads from both the forward flight and the maneuver flight conditions.

Upper Level Optimization

The upper level optimization consists of the general-purpose optimization program CONMIN (ref. 33) and an approximate analysis used to reduce the number of HOVT and CAMRAD/JA analyses during the iteration process. The approximate analysis is used to extrapolate the upper level objective function and upper level constraints with linear Taylor-series expansions using derivatives of the objective function and constraints with respect to the design variables

$$\text{OBJ} = \text{OBJ}_0 + \sum_{i=1}^{\text{NDV}} \left. \frac{\partial \text{OBJ}}{\partial \text{DV}_i} \right|_0 \Delta \text{DV}_i \qquad (11)$$

and

$$g = g_0 + \sum_{i=1}^{\text{NDV}} \left. \frac{\partial g}{\partial \text{DV}_i} \right| \Delta \text{DV}_i \qquad (12)$$

The assumption of linearity is valid over a suitably small change in the design-variable values and will not introduce a large error into the analysis provided that the changes ΔDV are small. Errors that may be introduced by use of the approximate analysis are controlled by imposing "move limits" on each design variable during the iteration process. A move limit that is specified as a fractional change of each design-variable value is imposed as an upper and lower design-variable bound. At the present time, the move limits are manually adjusted.

Lower Level Analysis and Optimization

This section of the paper describes the lower level analysis and lower level optimization procedure. The purpose of each lower level optimization is to assess whether a structure at the given radial location can be sized to provide the stiffnesses required by the upper level optimization and still have the strength to withstand loads calculated by the upper level

analysis. The lower level optimizations can be done in parallel because they are independent.

For simplicity, because closed-form equations can be derived (see appendix C), the structural member (fig. 5) is assumed to be a thin-walled isotropic box. The box cross section is symmetric about the horizontal axis with wall thicknesses (t_i) and lumped areas (a_j) which are analogous to longitudinal stringers in a wing box cross section. The outer dimensions b (the box beam width) and h (the box beam height) are functions of the upper level design variables because b and h depend on the local chord and the local airfoil thickness. The values of b and h are determined by placing a box of maximum area within the airfoil cross section by using the method of reference 34. (See appendix D.)

Lower Level Design Variables

The design variables are the three wall thicknesses $(t_1, t_2, \text{ and } t_4)$ and the three lumped areas $(a_1, a_2, \text{ and } a_3)$. The lumped areas are used to give the lower level more flexibility in matching the upper level stiffnesses. For the present implementation, the lumped areas are assumed to be square areas.

Lower Level Objective Function

The objective function is a measure of the difference between the stiffnesses required on the upper level and those determined from the lower design variables

$$F = \left[\frac{EI_{zz} - (EI_{zz})^*}{(EI_{zz})^*} \right]^2 + \left[\frac{EI_{xx} - (EI_{xx})^*}{(EI_{xx})^*} \right]^2 + \left[\frac{GJ - (GJ)^*}{(GJ)^*} \right]^2 \qquad (13)$$

where a starred quantity $(\ )^*$ denotes an upper level design variable. The lower level cross-sectional properties I_{xx}, I_{zz}, and J are computed (see appendix C), E is Young's modulus of elasticity, and G is the torsional modulus of elasticity.

Lower Level Constraints

The constraints are enforced on the extensional stiffness, stresses, and the physical dimensions of the wall thicknesses and lumped areas. The extensional stiffness constraint that requires the lower level calculated extensional stiffness EA (appendix C) to be equal or greater than the upper level extensional stiffness $(EA)^*$ (an upper level design variable) is given by

$$g_{c,i} = 1 - \frac{EA}{(EA)^*} \leq 0 \qquad (14)$$

at the given cross section. The extensional stiffness appears in a constraint rather than in the objective function (eq. (13)) where the other stiffnesses appear. This is done because the role of EA in the upper level is limited to satisfying the strain constraints (eq. (9)). The lower level is responsible only for assuring that the value of EA is at least as large as the value needed in the upper level; i.e., close matching of EA to $(EA)^*$ is not required.

The stress constraint evaluated at the corner of the box cross section shown in fig. 5 has the form

$$g_{c,i} = \frac{V(\sigma, \tau)}{\sigma_a} - 1 \leq 0 \qquad (15)$$

where σ is the bending stress, τ is the shear stress, and $V(\sigma, \tau)$ is the Von Mises stress measure. (See appendix C.) Two stress constraints are used: in one, τ is based on the vertical wall thickness, and in the other, τ is based on the horizontal wall thickness.

A set of constraints is imposed on the lower level wall thicknesses to assure that the section remains a thin-walled section and that the expression for J remains valid. (See appendix C.) These constraints are

$$g_{c,i} = \frac{t_j}{0.1b} - 1 \leq 0 \quad (j = 2 \text{ and } 4) \qquad (16)$$

$$g_{c,i} = \frac{t_j}{0.1h} - 1 \leq 0 \quad (j = 1 \text{ and } 3) \qquad (17)$$

where b and h are the width and height of the box cross section, respectively.

A set of constraints is imposed on the lumped areas and wall thicknesses that require that the dimensions are physically possible (i.e., that the lumped areas can fit inside the box cross section). These constraints are

$$g_{c,i} = -\left(\frac{b - t_4 - t_2}{2} - \sqrt{a_1} - \frac{1}{2}\sqrt{a_2}\right) \leq 0 \quad (18)$$

$$g_{c,i} = -\left(\frac{b - t_4 - t_2}{2} - \sqrt{a_3} - \frac{1}{2}\sqrt{a_2}\right) \leq 0 \quad (19)$$

$$g_{c,i} = -(h - t_1 - t_3 - 2\sqrt{a_1}) \leq 0 \qquad (20)$$

$$g_{c,i} = -(h - t_1 - t_3 - 2\sqrt{a_2}) \leq 0 \qquad (21)$$

$$g_{c,i} = -(h - t_1 - t_3 - 2\sqrt{a_3}) \leq 0 \qquad (22)$$

In addition, a set of constraints representing upper and lower bounds on the design variables is used.

For the kth design variable, the lower bound is given by

$$g_{c,i} = v_{k,l} - v_k \leq 0 \qquad (23)$$

and the upper bound is given by

$$g_{c,i} = v_k - v_{k,u} \leq 0 \qquad (24)$$

where $v_{k,l}$ and $v_{k,u}$ are the lower and upper design variable bounds, respectively.

For convenience, the set of lower level constraints defined by equations (14)–(24) is replaced by a single cumulative constraint, an envelope function known as the KS function (ref. 29), which approximates the active constraint boundary

$$KS = g_{max} + \frac{1}{\rho}\ln\left[\sum_{i=1}^{nc} e^{\rho(g_{c,i} - g_{max})}\right] \leq 0 \qquad (25)$$

where g_{max} is the maximum constraint component from equations (14)–(24), nc is the number of lower level constraint components, and ρ is defined by the user. Initially, ρ is small and then increases until a maximum value ρ_{max} is reached. For large values of ρ, the value of KS approaches g_{max}. The KS function is a single measure of the degree of constraint satisfaction or violation and is positive (violated) if at least one of the constraints $g_{c,i}$ is violated. The KS function is a single-valued function that is continuous and differentiable. This property becomes important when implementing the upper and lower levels as described in the section on the overall organization of the IADS procedure.

Lower Level Optimization Procedure

The flowchart for each lower level optimization procedure is shown in figure 6. Loads, local chord, box beam width, box beam height, and upper level stiffnesses are passed down from the upper level analysis. The lower level design variables (fig. 5) are used to calculate lower level stiffnesses. Von Mises stresses are calculated using the loads from the forward flight and maneuver analyses. The lower level objective function (eq. (13)) and cumulative constraint (eq. (25)) are evaluated. The lower level optimizations are performed using the general-purpose optimization program CONMIN. Exact analyses are used to evaluate the objective function, the constraint, and any gradients computed by CONMIN. The optimization process is converged when the objective function is minimized and the cumulative constraint is satisfied. After convergence, the process returns to the upper level.

Coordination Between Upper and Lower Levels

The coordination between upper and lower levels is implemented by upper level constraints. These constraints are imposed to encourage changes in the upper level design variables that promote consistency between the upper and lower level stiffnesses. Specifically, these constraints (one for each lower level optimization) have the form

$$g = F^U - (1 + \varepsilon)F_o^L \leq 0 \qquad (26)$$

where F_o^L is the most recent value of the lower level objective function (i.e., the optimum value of eq. (13)), F^U is an estimate of the change in F_o^L that would be caused by a change in the upper level design variable values, and ε is a specified tolerance defined as the coordination parameter. (See appendix A.) The importance of this parameter will be discussed later.

Equation (26) is the general form of the coordination constraint as formulated in reference 15. As shown in appendix A, the coordination constraint can be approximated in terms of the lower level total optimum sensitivity derivative that expresses how the optimum lower level objective function and lower level active constraint will change with a change in upper level design variable.

Overall Organization of IADS Procedure

The conceptual IADS procedure is shown in figure 2. It consists of an upper level analysis (fig. 3), three lower level optimizations (fig. 6), and a coordination task. The actual IADS procedure is more complicated and requires, in addition, an upper level sensitivity analysis and three lower level optimum sensitivity analyses.

The flowchart for the IADS procedure is shown in figure 7. First, the upper level analysis is executed for the current set of design variables providing all the information needed to calculate the upper level objective function and constraints with the exception of the coordination constraints. The upper level analysis also provides the loads, local chord, box beam width, box beam height, and stiffnesses (to be matched) to the lower level analysis. Each lower level optimization is performed to obtain a set of lower level design variables that match the current upper level bending and torsional stiffnesses as close as possible.

Next, an upper level sensitivity analysis is performed consisting of forward finite-difference derivatives (or gradients) of the upper level analysis. These derivatives are required to approximate the upper level objective function and upper level constraints during the upper level optimization. In addition, the loads and local chords corresponding to the changes in the upper design variables are saved. These quantities are used in the three lower level optimum sensitivity analyses to approximate the coordination constraint (eq. (26)). Appendix A describes how the coordination constraint is expressed in terms of the total optimum sensitivity derivative involving both changes in the optimum lower level objective function with respect to changes in the upper level design variables and changes in the active lower level constraint with respect to changes in the upper level design variables.

Finally, the upper level optimization occurs consisting of CONMIN and an approximate analysis. This describes 1 cycle of the IADS procedure. The process is repeated for additional cycles until convergence is achieved. A very strict convergence criterion is used for demonstration purposes. The overall procedure is converged when the change in the upper level objective function is less than 0.5×10^{-5} over three consecutive cycles and all the constraints (both upper and lower level) are satisfied. A step size of 0.001 is used to compute the finite-difference derivatives.

Demonstration of IADS Procedure

This section of the paper describes the analytical blade model, the mission definition, the optimization problem, and the optimization results used to demonstrate the IADS procedure. Results are presented for three studies: (1) the effect of initial design, (2) the effect of the coordination parameter ε, and (3) the comparison between a single-level and multilevel optimization approach.

Analytical Blade Model

The analytical blade model used to demonstrate the IADS procedure represents a wind tunnel model of a rotor blade for a four-bladed helicopter having a blade radius of 4.68 ft. Three sets of advanced rotorcraft (RC) airfoils are used along the blade: the RC(4)-10 airfoil (ref. 35) from the root to 85 percent radius, the RC(3)-10 airfoil (ref. 36) from 85 to 95 percent radius, and the RC(3)-08 airfoil (ref. 36) from 95 percent radius to the tip. Tables of experimental two-dimensional airfoil data for these three airfoil types are used in both HOVT and CAMRAD/JA. The analytical model of the blade uses 19 aerodynamic segments for HOVT, and it uses 50 structural segments and 18 aerodynamic segments for CAMRAD/JA. HOVT is used to predict

the power required in hover using nonuniform inflow (no wake is included) by trimming to a constant lift (C_L). CAMRAD/JA is used to predict rotor performance, loads, and frequencies using uniform inflow with empirical inflow correction factors for the forward and maneuver flight conditions. Uniform inflow is used to save on computational costs. (Note that even though an approximate analysis is used in the upper level optimization, 46 CAMRAD/JA analyses are required per optimization cycle.) In CAMRAD/JA an isolated rotor analysis is used that trims the rotor to constant lift (C_L) and drag (C_D) and zero flapping angle relative to the shaft using collective, lateral cyclic, and longitudinal cyclic pitch. From the modal analyses in CAMRAD/JA using 10 bending modes and 5 torsional modes, only the first 6 bending frequencies are below 10 per rev and need to be constrained for a four-bladed rotor. Because $f_{b,1}$ corresponds to a rigid-body mode and $f_{b,2}$ is the 1/rev frequency, the first two frequencies are not constrained. Constraints are placed on the first four bending frequencies ($f_{b,3}$, $f_{b,4}$, and $f_{b,6}$ are flapping dominated and $f_{b,5}$ is lead-lag dominated) and the first two torsional frequencies ($f_{t,1}$ represents the rigid-body torsional mode due to the control system stiffness and $f_{t,2}$ represents the first elastic torsional mode).

Mission Definition

The flight conditions are a constant lift of $1g$ (331 lb and $C_L = 0.0081$), a propulsive force of 32 lb ($C_D = -0.000811$), and an advance ratio of 0.35 for the forward flight condition and a constant lift of 401 lb ($C_L = 0.00985$), a propulsive force of 23 lb ($C_D = -0.000596$), and an advance ratio of 0.3 for the maneuver flight condition, which is for a load factor of 1.22. These flight conditions and the load factor are similar to those used in reference 37.

Optimization Problem

The objective function is a combination of the power required in hover, forward flight, and maneuver and of the 4/rev rotating vertical hub shear in forward flight. The objective function is chosen to be one dominated by performance with little emphasis on dynamics. Of the three powers, reducing the power required in hover is assumed to be the most important; it will have twice the weight as the other two powers. Several values were tried for the weighting factor on the hub shear term. To obtain the proper balance between performance and dynamics, k_4 must be between one and two orders of magnitude less than k_1. Thus, for this case, the weighting factors

are chosen to be $k_1 = 10, k_2 = k_3 = 5$, and $k_4 = 0.5$. Therefore, we have

$$\text{OBJ} = 10\frac{P_h}{P_{h,\text{ref}}} + 5\frac{P_{\text{ff}}}{P_{\text{ff,ref}}} + 5\frac{P_m}{P_{m,\text{ref}}} + 0.5\frac{S_{4,\text{ff}}}{S_{4,\text{ref}}} \quad (27)$$

where $P_{h,\text{ref}}, P_{\text{ff,ref}}, P_{m,\text{ref}}$, and $S_{4,\text{ref}}$ are 15 hp, 13 hp, 12 hp, and 2 lbf, respectively. The reference values are chosen to be representative of the powers required and the hub shear for all the initial blade designs used in this work.

The upper and lower bounds for the design variables are given in table 1. On the upper level, 22 design variables and 95 constraints are used. On the lower level, 6 design variables and 1 cumulative constraint (the KS function with 24 components) are used at each of the 3 spanwise locations (i.e., the root, the point of taper initiation, and the tip).

Parameters and flight conditions are summarized in table 2. Because the blade is made of aluminum, E has a value of 15.26×10^8 lb/ft^2, the allowable strain ε_a has a value of 0.05 ft/ft, and the allowable stress σ_a is 8.352×10^6 lb/ft^2. The values for minimum tip chord ($c_{t,\text{min}}$), power available (P_a), minimum autorotational inertia, and maximum allowable drag coefficient ($c_{d,\text{all}}$) are 0.083 ft, 20 hp, 23.69 lbm-ft^2, and 0.12, respectively. Frequencies must be at least 0.1 away from a per-rev value ($\Delta f = 0.1$/rev in eq. (6)).

Study on Effect of Initial Designs

The IADS multilevel optimization procedure is demonstrated for three examples using the three starting points shown in figure 8. Example 1 (fig. (8a)) uses a rectangular planform with a pretwist of $-9°$, a root chord of 0.3449 ft, and upper level stiffness design variables initialized to be consistent with the lower level initial wall thickness and lumped areas (i.e., matched stiffnesses). Example 2 (fig. (8b)) uses a tapered planform with a pretwist of $-16°$, a root chord of 0.45 ft, and matched stiffnesses. The blade is rectangular to 80 percent radius and then tapers linearly to the tip with a 3-to-1 taper ratio. Example 3 (fig. (8c)) uses the same planform and pretwist as example 2 except that the upper and lower level stiffnesses are unmatched. All these examples use a value of -0.4 for the coordination parameter (ε) in equation (26). The importance of the choice of ε is examined in a later section of the paper.

Example 1: rectangular planform ("initially matched stiffnesses"). The starting point for the optimization is the rectangular blade shown in figure 8(a). The upper and lower level stiffnesses are matched because the upper level stiffnesses are

started with the stiffnesses determined by the initial lower level design variables. This is an infeasible starting point because the lower level stress constraints at the root are violated. (See the results given in table 3.) The initial and final values for the blade planform, performance measures, and dynamics measures are given in table 3(a). The initial and final values for the constrained frequencies are given in table 3(b). Notice that the final value for the fourth bending frequency $f_{b,4}$ is in a different frequency range than the initial value. Final values for the lower level design variables and the upper level stiffnesses are given in table 3(c). The final design is able to improve the performance characteristics from the initial blade and satisfy all the constraints. Compared with the initial values, the final design represents a 2.1-, 2.3-, 2.3-, 47.6-, and 3.2-percent reduction in the power required in hover, forward flight, and maneuver; hub shear; and upper level objective function, respectively.

The final stiffness distributions for the upper (required values) and lower levels (actual values) are shown in figure 9. The matching of the chordwise bending stiffness (EI_{xx}) (fig. 9(a)), the flapwise bending stiffness (EI_{zz}) (fig. 9(b)), and the torsional stiffness (GJ) (fig. 9(c)) are extremely good. As shown in figure 9(d), the lower level is able to obtain an extensional stiffness distribution higher than the minimum requirement set by the upper level.

Convergence histories of the individual terms of the lower level objective function (eq. (13)) are shown in figure 10 for the three locations: the root (fig. 10(a)), the point of taper initiation (fig. 10(b)), and the tip (fig. 10(c)). Each term (denoted stiffness deviation) is a measure of how well the upper and lower stiffnesses match. Initially, the stiffnesses are matched, but the stress constraints are violated at the root. Therefore, the lower level design variables must change to satisfy these constraints while keeping the upper and lower level stiffnesses matched as close as possible. Notice that the chordwise stiffness at the root, the torsional stiffness at the point of taper initiation, and the flapwise stiffness at the tip are the last stiffnesses to match. Further, it appears that stiffnesses at the point of taper initiation are particularly difficult to match. This difficulty may be due to the fact that the point of taper initiation is a design variable but the root and tip positions are fixed.

The reason for the deviations in the stiffness is that the upper and lower levels are in conflict. One component of the upper level objective function is the hub shear which can be reduced significantly by increasing the blade stiffnesses. On the upper

level, if the optimizer did not have to be concerned with stiffness matching, it would increase the upper level stiffnesses. Without the lower level to keep the stiffnesses in check, a heavy or nonbuildable blade might result.

The information shown in figure 10 is collected and used to determine when a move-limit adjustment is necessary for an upper level design variable during the overall optimization process. (Recall that an approximate analysis is used on the upper level and an exact analysis is used on the lower level.) At the present time, no automatic move-limit adjustment is used in the approximate analysis on the upper level. Instead, the IADS procedure is run for 8 cycles and then the stiffness deviations are examined. When the stiffness deviation increases (e.g., cycle 16), the design-variable move limits are manually reduced and the optimization process is continued for another 8 cycles. In practical applications, the optimization procedure would terminate after about 30 cycles; however, for demonstration purposes, the convergence criterion is set to a very small value. Both the upper and lower levels have the same tight convergence criterion on each cycle. Overall convergence of the IADS procedure might improve if the convergence criterion is relaxed initially and then tightened as the optimization proceeds.

Example 2: tapered planform ("initially matched stiffnesses"). The starting point for the optimization is the tapered blade shown in figure 8(b). Initially, the upper and lower level stiffnesses are matched because the upper level stiffness is determined by the lower level design variables. However, this is an infeasible starting point because a thin-wall-theory constraint is violated on the lower level. The initial and final values for the blade planform, performance measures, and dynamics measures are given in table 4(a). The initial and final constrained frequencies are included in table 4(b). The final design is able to improve the performance characteristics from the initial blade. However, the hub shear increases from the initial value.

Figure 11 shows the final stiffness distributions for the upper levels (required values) and lower levels (actual values) for the chordwise bending stiffness (fig. 11(a)), flapwise bending stiffness (fig. 11(b)), and torsional stiffness (fig. 11(c)). As shown in the figure, the stiffness matching is good, although not as good as in example 1. The lower level is able to obtain an extensional stiffness distribution (fig. 11(d)) higher than the minimum requirement.

Figure 12 shows stiffness deviation versus cycle number for the three matching locations: the root

11

(fig. 12(a)), the point of taper initiation (fig. 12(b)), and the tip (fig. 12(c)). Early in the optimization process, the flapwise and torsional stiffnesses are both unmatched. After cycle 10, the matchings improve, and after 25 cycles, all three matchings are good. At the tip (fig. 12(c)), matching proves to be quite difficult. The torsional stiffness is the last to match. The reason for this is that the blade initial design is tapered, and it is difficult to place a thin-wall section in the space near and at the tip and still match the stiffness required on the upper level.

Example 3: tapered planform ("initially unmatched stiffnesses"). In the previous examples, the starting points used matched stiffnesses. The purpose of the present example is to demonstrate how the IADS procedure behaves when it is started from an inconsistent set of stiffnesses (i.e., unmatched stiffnesses). The starting point for the optimization is shown in figure 8(c). The initial stiffnesses used in the upper level are much larger than the stiffnesses obtained from the lower level design variables. The initial and final values for the blade planform, performance measures, and dynamics measures are given in table 5(a). The initial and final constrained frequencies are included in table 5(b). The final upper and lower level stiffnesses are shown in figure 13, which also shows that the optimization procedure is able to match the upper and lower level stiffnesses successfully. Figure 14 shows the stiffness deviations for the three matching locations: the root (fig. 14(a)), the point of taper initiation (fig. 14(b)), and the tip (fig. 14(c)). As shown in the figure, the optimization procedure is able to match all three stiffnesses after 25 cycles, but it is at the expense of upper level performance. (See table 5.) The power required for all three flight conditions has increased substantially along with the hub shear. Notice that a bending frequency $f_{b,6}$ has shifted frequency intervals. From these results it appears that although the optimization procedure will converge when starting from an initial point that has unmatched stiffnesses, starting with a set of consistent stiffnesses is better.

Observations on Effect of Initial Design Study

The IADS procedure has been exercised for three starting blade planforms: a rectangular planform with matched stiffnesses, a tapered planform with matched stiffnesses, and a tapered blade with unmatched stiffnesses. In all cases, the procedure is able to find converged feasible designs. When comparing examples 1 and 2 (tables 3 and 4, respectively), the reader will find two different final blade designs (i.e., the design variable values are different) with essen-

tially the same objective function value. Apparently, many different combinations of design variables exist that satisfy the matching constraints, and more than one of these is optimal. The final solution depends on initial conditions. In example 3 (table 5), the optimizer appears to converge to a suboptimal solution when compared with example 2. Both examples started from the same planform, but example 2 starts with matched stiffnesses and example 3 starts with unmatched stiffnesses. Because the initial matching of the stiffnesses is relatively easy, this suggests that the initial matching should always be enforced.

When comparing all three examples, the reader will also notice that each initial blade has a different frequency range for the bending and torsional frequencies and that each final blade design has a frequency which has shifted a frequency interval (e.g., $f_{b,6}$ in example 3). During the approximate analysis, the optimizer can change the upper level design variables such that a frequency can shift intervals. However, as the design-variable move limits are reduced, this shifting is less likely to occur.

At the present time, no automatic move-limit adjustment is used in the upper level approximate analysis. However, the stiffness deviation information (e.g., fig. 10) can be collected and used to determine when a move-limit adjustment is necessary for an upper level design variable during the overall optimization process.

Study on Effect of Coordination Parameter ε

The purpose of this study is to demonstrate the effect of ε in the coordination constraint (eq. (26)) on the optimization procedure. Results for three values of ε (0.4, -0.2, and -0.4) are presented in table 6 and figures 15, 16, and 9, respectively. If ε is a large positive value, the levels are essentially independent. The upper level is free to change the upper level stiffness and chord distributions in any way that will reduce the upper level objective function. The only requirement is that the overall stiffness matching should not degrade by more than the value of ε from the best match found on the last lower level optimization. For example, if $\varepsilon = 0.4$, the stiffness matching can degrade by 40 percent and still satisfy the coordination constraints. Therefore, the procedure could possibly converge with the upper and lower level stiffnesses being mismatched by as much as 40 percent. A negative value for ε means that the upper level must improve the matching achieved on the lower level by that amount. This section of the paper presents results for several values

of ε using the starting point in figure 8(a) that is also used in example 1.

One choice for ε would be zero. This would mean that the upper level cannot degrade the matching achieved on the lower level. This value was found to be too restrictive for the optimization process, and the procedure converged in 3 cycles with very little change in the upper level design variables. The reason for this can be seen by examining the coordination constraint (eq. (26)). At the start of the upper level optimization, the coordination constraint at each matching location is active (i.e., $g = 0$) because F^U is equal to F_o^L. As the upper level optimizer tries to change the upper level design variables, the coordination constraints become violated. Therefore, the upper level optimizer makes only small changes and the process converges in 3 cycles.

As shown in table 6, when $\varepsilon = 0.4$, the optimization process is able to improve the performance and dynamics measures over the initial blade values and improve the lower level (i.e., satisfy the stress constraints). This improvement is achieved at the expense of stiffness matching. Figure 15 shows the final stiffness distributions for the upper and lower levels. The lower level is not able to find a set of stiffnesses to match those required by the upper level. This final result is technically a feasible design because all the constraints are satisfied. Recall that the upper and lower stiffnesses need only be as close as possible (lower level objective function). The upper level coordination constraints do not require the upper and lower level stiffnesses to match exactly.

When $\varepsilon = -0.2$, the optimization procedure is able to obtain a design that has some improvement over the initial starting point (table 6). The upper level objective function is reduced slightly, but not as much as when ε is positive. As shown in figure 16, the upper and lower stiffnesses match well for the chordwise stiffness (fig. 16(a)), the flapwise stiffness (fig. 16(b)), and the torsional stiffness (fig. 16(c)). The lower level is able to obtain an extensional stiffness which is slightly larger than that required by the upper level.

Of the values used in this work, the best value for ε is -0.4 because the optimization procedure is able to obtain improvement on the upper level and find a set of consistent stiffnesses on the lower level. These results (example 1) are included in table 6 for completeness. The stiffness distributions are shown in figure 9.

Observations on Effect of Coordination Parameter ε Study

As shown previously, positive values of ε result in upper level improvement, but poor stiffness matching and negative values of ε result in both upper level improvement (although not quite as good as when ε is positive) and good stiffness matching. This suggests that a gradual reduction in ε from a positive value to a negative value could be beneficial. The IADS procedure was run with $\varepsilon = 0.4$ for 8 cycles, $\varepsilon = 0.2$ for 8 cycles, $\varepsilon = -0.2$ for 8 cycles, and $\varepsilon = -0.4$ for 8 cycles. This technique of gradually reducing the value of ε did not work. Presumably, the upper level planform area and upper level stiffnesses increased to improve the upper level objective function when ε was positive so that by the time that ε was negative, the stiffness matching was achieved at the expense of performance and dynamic improvement on the upper level. This situation is analogous to example 3 in which the mismatched initial conditions resulted in stiffness matching at the expense of upper level improvement.

Study on Comparison of Two-Level and Single-Level Optimization Procedures

The IADS procedure is compared with a more traditional optimization procedure without multilevel decomposition (i.e., the single-level optimization procedure). The single-level optimization procedure combines local and global design variables and simultaneously evaluates aerodynamics, dynamics, and structures. The design variables are the same as those used in the IADS procedure with the exception of the stiffness design variables (EI_{xx}, EI_{zz}, GJ, and EA) which are no longer needed. These stiffnesses are calculated from the wall thicknesses, the lumped areas, and the blade planform. The constraints are the same constraints used in the IADS procedure with two exceptions. First, the coordination constraints are no longer needed because the stiffnesses are calculated from the design variables. Second, the cumulative constraint, (KS), (eq. (25)) is no longer needed and the individual constraint components (eqs. (14)–(24)) are used. The single-level optimization procedure has 28 design variables and 218 constraints (eqs. (2)–(11) and (14)–(24)). The optimizer consists of CONMIN and an approximate analysis. All derivatives are calculated by forward finite differences and results are presented for four cases. Cases 1 and 2 compare the single-level and multilevel approaches using the initial designs in figures 8(a) and 8(b), respectively. Cases 3 and 4 investigate whether the multilevel approach can improve on the best solutions found by the single-level

approach. All the IADS cases use a value of -0.4 for the coordination parameter (ε).

Case 1: rectangular starting design. The starting point for case 1 is shown in figure 8(a), and initial and final results for the two approaches are given in table 7. Both approaches show improvement over the initial design. The single-level approach finds a better overall design in terms of the objective function than the multilevel approach and is faster to converge. The multilevel approach has slightly less performance improvement but more dynamics improvement than the single-level approach.

Case 2: tapered starting design. The starting point for case 2 is the tapered blade shown in figure 8(b). Initial and final results for the two approaches are given in table 8. For this starting point, only the multilevel approach converges to a feasible design. The single-level approach was manually discontinued after 64 cycles. The final single-level design includes large lumped masses resulting in a weight constraint that is grossly violated ($W = 4.4$ lb).

Case 3: starting from feasible single-level design. The purpose of case 3 is to see if the IADS optimization procedure can improve on the best solution obtained by a single-level optimization procedure. The initial design for the multilevel procedure is rectangular to 0.7131 percent radius and then tapers linearly to the tip with a taper ratio of 2.21 to 1. This is the best solution found using the single-level approach in case 1 (table 1). The results are given in table 9. The multilevel approach is able to improve the design only slightly over that obtained by the single-level approach.

Case 4: starting from infeasible single-level design. Recall in case 2 that the single-level approach did not find a feasible design although the IADS procedure did find a feasible design. The purpose of case 4 is to see if the IADS optimization procedure can start from that final infeasible single-level solution (table 8) and obtain a feasible design. Thus, the initial design for the multilevel procedure has a pretwist of $-13.22°$ and a planform that is rectangular to 0.4934 percent radius and then tapers linearly to the tip with a taper ratio of 3.098 to 1 with a root chord of 0.4899 ft. The IADS procedure is able to find a feasible design, and the initial and final results are given in table 10. The final upper and lower level stiffness distributions for the three matching locations are shown in figure 17 and the stiffness deviations are shown in figure 18.

Observations on multilevel versus single-level optimization cases. The IADS procedure is compared with a more traditional optimization procedure without decomposition (single-level optimization procedure) for four cases. In the first and second cases, the initial design had a rectangular planform and a tapered planform, respectively. In the third and fourth cases, the IADS procedure is started with the best designs from a single-level optimization procedure. The multilevel optimization approach is able to find feasible final designs regardless of the initial planform design. The single-level optimization procedure could find only a feasible final design when the initial planform was rectangular (case 1). When the initial planform was tapered (case 2), the single-level optimization procedure could not find a feasible design and was terminated manually because the blade weight constraint was grossly violated. In cases 3 and 4, the multilevel approach was started from two single-level optimization results of cases 1 and 2, respectively. In case 3, the multilevel approach improved the single-level design slightly. In case 4, the initial design for the IADS procedure is the infeasible single-level design that has a grossly violated weight constraint. The IADS procedure is able to start with this highly infeasible design and find a feasible design.

Concluding Remarks

An integrated aerodynamic/dynamic/structural (IADS) optimization procedure for helicopter rotor blades has been developed. The procedure combines performance, dynamics, and structural analyses with a general-purpose optimizer using multilevel decomposition techniques. At the upper level, the structure interacts with the disciplines of aerodynamics and dynamics in terms of global quantities (stiffnesses and average strains). At the lower level, the structure is defined in terms of local quantities (detailed dimensions of the blade structure and stresses).

The IADS procedure consists of an upper level optimization, a lower level optimization, and a coordination task. The upper level objective function is a linear combination of performance and dynamic measures. Upper level design variables include pretwist, point of taper initiation, taper ratio, root chord, blade stiffnesses, tuning masses, and tuning mass locations. Upper level constraints consist of limits on power required in hover, forward flight, and maneuver; airfoil drag; minimum tip chord; trim; blade natural frequencies; autorotational inertia; blade weight; and average strains.

The lower level optimization sizes the internal blade structure to provide the stiffnesses required by the upper level and assure the structural integrity of

the blade. The lower level design variables are the box beam wall thicknesses and several lumped areas that are analogous to longitudinal stringers in a wing box cross section. The lower level objective function is a measure of the difference between the upper level stiffnesses and the stiffnesses computed from the wall thicknesses and lumped areas. The lower level constraints are on Von Mises stresses, extensional stiffnesses, thin-wall theory, and dimensional limits.

The coordination task consists of a set of upper level constraints that link the levels and promote consistency between the upper and lower level stiffnesses. A coordination parameter is included in each constraint. This parameter specifies the amount of coupling between the levels. A proper value for the coordination parameter is found to be crucial to the success of the IADS procedure. If the parameter has a positive value, the procedure will converge but the final stiffness matching can be unacceptable. If the parameter value is too small (approximately zero), the optimization process will terminate without improving the dynamics or performance measures. A small negative value for the coordination parameter encourages the upper level to improve dynamics and performance using stiffness values that the lower level can match.

The IADS procedure is demonstrated by using a model-size rotor blade for several initial blade planforms and varying amounts of coupling between the levels. In addition, the IADS multilevel procedure is compared with a more traditional optimization procedure without decomposition (a single-level optimization procedure). In all cases, the IADS procedure achieves successful results. It converges to a feasible design regardless of whether the initial design had a set of consistent stiffnesses. However, initializing the upper level stiffnesses with the stiffnesses calculated from the lower level design variables greatly improves the final design. For the cases studied, the IADS procedure is found to be superior to the single-level optimization procedure. The IADS procedure converges to a feasible design, even when the single-level procedure does not. Furthermore, the IADS procedure improves upon the best design found by the single-level optimization procedure.

The IADS procedure exploits the couplings and interactions between the disciplines of aerodynamics, dynamics, and structures. It provides an efficient method to integrate structures and/or structural properties into an optimization procedure because it guarantees that a structure with a consistent set of structural properties can be found. The IADS procedure provides an optimization technique that is compatible with industrial design practice in which the aerodynamic and dynamic design is performed at a global level and the structural design is carried out at a detailed level with considerable dialogue and compromise among the groups.

Appendix A

Coordination Constraint

In a multilevel decomposition approach, the coupling between levels is done through a coordination procedure (e.g., refs. 20 and 25). In the present work, the coordination procedure based on reference 20 is used to reconcile the stiffnesses required on the upper level with the stiffnesses that the lower level can actually obtain. This reconciliation results in one upper level constraint at each matching location

$$g = F^U - (1 + \varepsilon)F_o^L \leq 0 \qquad (A1)$$

where F_o^L is the most recent value of the lower level objective function (i.e., the optimum value of eq. (13)), F^U is an estimate of the change in F_o^L that would be caused by a change in the upper level design variable values, and ε is the coordination parameter. This coordination parameter specifies how much the upper level can either degrade or improve the overall stiffness matching achieved on the lower level, and it may also be interpreted as a measure of how closely coupled the two levels are. If ε has a positive value, the two levels are not closely coupled (i.e., they are essentially independent). The upper level can change the upper level stiffness and chord distributions in any way that will improve the upper level objective function as long as the stiffness matching is not degraded by more than the amount of ε. If ε has a negative value, the two levels are closely coupled and the upper level is commanded to improve the matching by the amount of ε.

Equation (A1) is the general form of the coordination constraint as formulated in reference 15. The form of the coordination constraint used in this work is obtained by approximating F^U in terms of the current optimum lower level objective function (F_o^L). If F_o^L is expanded in terms of a first-order Taylor series about the lower level optimum, then F^U can be approximated by

$$F^U = F_o^L + \sum_{i=1}^{NDV} \left.\frac{dF^L}{dDV_i}\right|_0 \Delta DV_i \qquad (A2)$$

where DV_i is an upper level design variable and $\left.\dfrac{dF^L}{dDV_i}\right|_0$ is the total optimum sensitivity derivative

(ref. 28) given by

$$\left.\frac{dF^L}{dDV_i}\right|_0 = \left.\frac{\partial F^L}{\partial DV_i}\right|_0 - \lambda^T \left.\frac{\partial KS}{\partial DV_i}\right|_0 \qquad (A3)$$

where $\partial F^L/\partial DV_i$ is the derivative of the optimum lower level objective function with respect to the upper level design variables, $\partial KS/\partial DV_i$ is the derivative of the active lower level constraint (eq. (25)) with respect to the upper level design variables, λ^T is the Lagrange multiplier given by

$$\lambda^T = - \left[\left(\frac{\partial KS}{\partial v}\right)^T \left(\frac{\partial KS}{\partial v}\right) \right]^{-1} \left.\frac{\partial F^L}{\partial v}\right|_0 \qquad (A4)$$

where $\partial KS/\partial v$ is the vector of derivatives of the active lower level constraints with respect to the lower level design variables at the lower level optimum. At a lower level optimum, λ^T will be positive, and if no lower level constraint is active, λ^T is set to zero. By substituting equation (A2) into equation (A1), the coordination constraint g is approximated by

$$g = \left(F_o^L + \sum_{i=1}^{NDV} \left.\frac{dF^L}{dDV_i}\right|_0 \Delta DV_i \right) - (1 + \varepsilon)F_o^L \leq 0$$
$$(A5)$$

or simplifying gives

$$g = \left(\sum_{i=1}^{NDV} \left.\frac{dF^L}{dDV_i}\right|_0 \Delta DV_i \right) - \varepsilon F_o^L \leq 0 \qquad (A6)$$

From substituting equation (A3) into equation (A6), the coordination constraint becomes

$$g = \left[\sum_{i=1}^{NDV} \left(\left.\frac{\partial F^L}{\partial DV_i}\right|_0 \Delta DV_i - \lambda^T \left.\frac{\partial KS}{\partial DV_i}\right|_0 \right) \right] - \varepsilon F_o^L \leq 0$$
$$(A7)$$

which is the form implemented in this work.

The derivative of the coordination constraint is obtained by differentiating equation (A7) with respect to upper level design variables. Thus,

$$\frac{\partial g}{\partial DV_i} = \left.\frac{\partial F^L}{\partial DV_i}\right|_0 \qquad (A8)$$

Appendix B

Drag Constraints

Rotor blades operate over a wide range of flight conditions: hover, low-speed forward flight, high-speed forward flight, and maneuver. In addition, the blade encounters different conflicting phenoma as it rotates. Figure 19 shows a top view of the rotor disk with the advancing side when the blade is between $\Psi = 0°$ and $180°$ and with the retreating side when the blade is between $\Psi = 180°$ and $360°$. On the advancing side, the blade encounters a higher net velocity than it does on the retreating side where an area exists in which the flow is reversed. This reversed-flow region does not contribute any lift on the blade. In this work and in previous work (refs. 3, 4, and 14), aerodynamic concerns such as drag divergence and blade stall are expressed in terms of constraints on the drag coefficient at various azimuth angles (Ψ).

On the advancing side of the blade, c_d is checked at every spanwise station. The constraint is formulated so that the largest c_d is less than a given value of $c_{d,\text{all}}$. At a given azimuth angle, the largest section drag coefficient $c_{d,\text{max}}^{\Psi}$ is selected from the aerodynamic stations along the blade span. (See fig. 20.) Thus,

$$c_{d,\text{max}}^{\Psi} = \max(c_{d,1}, c_{d,2}, \ldots, c_{d,\text{MRA}})$$
$$(\Psi = 0°, 15°, 30°, \ldots, 180°) \quad \text{(B1)}$$

where $c_{d,i}$ is the section drag coefficient in the ith aerodynamic segment and MRA is the total number of aerodynamic segments.

Similarly, on the retreating side of the blade, c_d is constrained at each Ψ. The difference is caused by the reverse-flow region which occurs on the retreating side of the blade, and this must not be considered. In the reverse-flow region, c_d is large because of the reversed flow. The velocities in this region have a tangential velocity similar to the advance ratio. Therefore, on the retreating side of the blade at a given azimuth angle, the largest drag coefficient is give by

$$c_{d,\text{max}}^{\Psi} = \max(c_{d,k}, c_{d,k+1}, \ldots, c_{d,\text{MRA}})$$
$$(\Psi = 180°, 195°, 210°, \ldots, 360°) \quad \text{(B2)}$$

where $c_{d,k}$ is the first drag coefficient corresponding to the first value of $c_{l,k}$ outside the reverse-flow region as shown in figure 21.

At a given azimuth angle, the constraint is formulated as

$$g = \frac{c_{d,\text{max}}^{\Psi}}{c_{d,\text{all}}} - 1 \leq 0 \quad \text{(B3)}$$

where $c_{d,\text{all}}$ is the allowable drag coefficient and $c_{d,\text{max}}^{\Psi}$ is given by equations (B1) or (B2). Because several airfoils may be used along the blade, a composite $c_{d,\text{all}}$ is used. Different values of $c_{d,\text{all}}$ could be used for the advancing and retreating side constraints, but in this work the same value of 0.12 is used.

Appendix C

Lower Level Structural Analysis

The purpose of this appendix is to summarize the elementary equations describing the geometric and structural analysis for the lower level structure. A typical cross section of the thin-walled isotropic box section is shown in figure 5. For simplicity, the top and bottom wall thicknesses, t_1 and t_3, respectively, are equal. The total cross-sectional area (A) is the sum of the cross-sectional areas of the box beam elements A_i and the lumped areas a_j (described in the main text). Thus,

$$A = \sum_{i=1}^{n} A_i + \sum_{j=1}^{m} a_j \qquad \text{(C1)}$$

By using the familiar relations, the centroid of the cross section is calculated from the equations

$$x_c = \frac{\sum_{i=1}^{n} A_i x_i + \sum_{j=1}^{m} a_j x_j}{A} \qquad \text{(C2)}$$

and

$$z_c = \frac{\sum_{i=1}^{n} A_i z_i + \sum_{j=1}^{m} a_j z_j}{A} \qquad \text{(C3)}$$

where x_i and z_i are coordinates in the chordwise and flapwise directions, respectively, that specify the distance of the centroid of the ith element area (A_i) from the reference x- and z-axes shown in figure 5. Similarly, x_j and z_j are coordinates that specify the distance of the centroid of the jth lumped area (a_j) from the reference axes, n is the number of elements that the cross section is divided into for ease of calculations, and m is the number of lumped areas.

Next, the area moments of inertia of each element about its centroidal x- and z-axes are calculated from

$$I_{x,k} = \frac{b_k h_k^3}{12} \quad (k = 1, 2, \ldots, n + m) \qquad \text{(C4)}$$

$$I_{z,k} = \frac{h_k b_k^3}{12} \quad (k = 1, 2, \ldots, n + m) \qquad \text{(C5)}$$

where b_k is the base of the kth rectangular element, h_k is the height relative to the x-axis, and $I_{zz,i} = 0$ for symmetric elements. By using the parallel-axis theorem, the moments of inertia of each element are

found with respect to the centroid of the box beam as

$$\left. \begin{array}{l} I_{cx,k} = I_{x,k} + A_k d_k^2 \\ I_{cz,k} = I_{z,k} + A_k c_k^2 \end{array} \right\} \qquad \text{(C6)}$$

where $I_{cx,k}$ and $I_{cz,k}$ are the moments of inertia of the kth element about the centroid of the box beam, $I_{x,k}$ and $I_{z,k}$ are the moments of inertia of the kth element about its centroidal axes, and d_k and c_k are the distances from the centroid of the element to the centroid of the box beam in the x- and z-directions, respectively. The total moments of inertia for the box beam are equal to the sum of the element inertias:

$$\left. \begin{array}{l} I_{xx} = \sum I_{cx,k} \\ I_{zz} = \sum I_{cz,k} \end{array} \right\} \qquad \text{(C7)}$$

The polar moment of inertia (J) for the box beam is calculated by using the method described in reference 38 which gives

$$J = \frac{4A_c^2}{\oint ds/t} \qquad \text{(C8)}$$

where A_c is the enclosed area of the mean periphery of the box beam wall, ds is the differential circumferencial length along the box beam, and t is the local thickness of the wall.

In order to calculate the lower level objective function, the bending and torsional stiffnesses of the box beam are necessary. For an isotropic beam, the moments of inertia I_{xx} and I_{zz} calculated in equation (C7) are multiplied by Young's modulus E to acquire the bending stiffnesses EI_{xx} and EI_{zz} in the chordwise and flapwise directions, respectively. Similarly, the polar moment of inertia is multiplied by the torsional modulus of elasticity G to acquire the torsional stiffness of the beam GJ.

The stresses for the constraints in the lower level optimization are evaluated at the corners of the box beam by using the Von Mises stress measure given by

$$V(\sigma, \tau) = \sqrt{\sigma^2 + 3\tau^2} \qquad \text{(C9)}$$

where σ is the axial bending stress at the outer fiber of the cross section, which is given by

$$\sigma = \left(\frac{M_{zz}}{I_{zz}} \right) x_{\text{outer}} + \left(\frac{M_{xx}}{I_{xx}} \right) z_{\text{outer}} + \frac{\text{CF}}{A} \qquad \text{(C10)}$$

and τ is the shear stress due to torsion in the wall of the section with thickness t, which is given by

$$\tau = \frac{M_T}{2A_c t} \qquad \text{(C11)}$$

where M_{zz} is the flapwise moment, M_{xx} is the lag moment, CF is the centrifugal force, and M_T is the torque at the section. The shear stress due to transverse loads has been neglected for simplicity.

Here, M_{zz}, M_{xx}, N, and M_T are computed in the upper level analysis for forward flight and maneuver, multiplied by a factor of safety (l_f), and then passed to the lower level.

Appendix D

Wing Box Fitting

At a given radial location, the outer dimensions of the box cross section are determined by placing a rectangular box of maximum area within the given airfoil cross section using a modified version of the method described in reference 34. As shown in figure 22, the outer dimensions (where $\bar{b}$ denotes the nondimensional box beam width and $\bar{h}$ denotes the nondimensional box beam height) depend on the airfoil section and the local chord c. (Note that the upper coordinates $\bar{z}_u$, lower coordinates $\bar{z}_l$, horizontal coordinates $\bar{x}$, and maximum thickness location t_{max}, which are all normalized with respect to the chord c, are given in ref. 35 for the RC(4)-10 airfoil and in ref. 36 for the RC(3)-08 and RC(3)-10 airfoils.)

The procedure for the wing box fitting is described below, and the nondimensional box beam height ($\bar{h}$) is determined first. By starting from the leading edge of the airfoil at an initial point $\bar{x}_l$, which is given as

$$\bar{x}_l = \frac{t_{max}}{5} \tag{D1}$$

$\bar{z}_u^i$ and $\bar{z}_l^i$ are determined by linearly interpolating between the respective upper and lower airfoil coor-

dinates. The nondimensional box beam height ($\bar{h}$) is given by

$$\bar{h} = \bar{z}_u^i - \bar{z}_l^i \tag{D2}$$

Next, by starting at a distance $\bar{x}_r$, where

$$\bar{x}_r = 1 - \left(\frac{1 - t_{max}}{5} \right) \tag{D3}$$

the location of the right side of the box is similarly determined. If the box is not within the airfoil shape, $\bar{x}_r$ is increased from the trailing edge until the box is within the airfoil shape. The nondimensional box beam length ($\bar{b}$) is given by

$$\bar{b} = \bar{x}_r - \bar{x}_l \tag{D4}$$

and the nondimensional area $\bar{A}$ of the box is given by

$$\bar{A} = \bar{b}\bar{h} \tag{D5}$$

Next, $\bar{x}_l$ is incremented by 1 percent and the process is repeated to compute a new area. The larger of the two areas is kept. The process is repeated until three consecutive areas are within a given tolerance. When this occurs, a rectangular box of maximum area has been determined.

References

1. Miura, Hirokazu: *Applications of Numerical Optimization Methods to Helicopter Design Problems: A Survey.* NASA TM-86010, 1984.

2. Bennett, Richard L.: Application of Optimization Methods to Rotor Design Problems. *Vertica*, vol. 7, no. 3, 1983, pp. 201–208.

3. Walsh, Joanne L.; Bingham, Gene J.; and Riley, Michael F.: Optimization Methods Applied to the Aerodynamic Design of Helicopter Rotor Blades. *J. American Heli. Soc.*, vol. 32, no. 4, Oct. 1987, pp. 39–44.

4. Walsh, Joanne L.: *Performance Optimization of Helicopter Rotor Blades.* NASA TM-104054, 1991.

5. Nixon, Mark W.: *Preliminary Structural Design of Composite Main Rotor Blades for Minimum Weight.* NASA TP-2730, AVSCOM TM-87-B-6, 1987.

6. Friedmann, P. P.; and Shanthakumaran, P.: Optimum Design of Rotor Blades for Vibration Reduction in Forward Flight. *Proceedings of the 39th Annual Forum of the American Helicopter Society,* May 1984, pp. 656–673.

7. Peters, David A.; Ko, Timothy; Korn, Alfred; and Rossow, Mark P.: Design of Helicopter Rotor Blades for Desired Placement of Natural Frequencies. *Proceedings of the 39th Annual Forum of the American Helicopter Society,* 1983, pp. 674–689.

8. Davis, Mark W.; and Weller, William H.: Application of Design Optimization Techniques to Rotor Dynamics Problems. *J. American Heli. Soc.*, vol. 33, no. 3, July 1988, pp. 42–50.

9. Celi, R.; and Friedmann, P. P.: Efficient Structural Optimization of Rotor Blades With Straight and Swept Tips. *Proceedings of the 13th European Rotorcraft Forum,* Sept. 1987, Paper No. 3-1.

10. Friedmann, Peretz P.: Impact of Structural Optimization With Aeroelastic/Multidisciplinary Constraints on Helicopter Rotor Design. AIAA-92-1001, Feb. 1992.

11. Adelman, Howard M.; and Mantay, Wayne R., eds.: *Integrated Multidisciplinary Optimization of Rotorcraft: A Plan for Development.* NASA TM-101617, AVSCOM TM-89-B-004, 1989.

12. Adelman, Howard M.; and Mantay, Wayne R.: Integrated Multidisciplinary Design Optimization of Rotorcraft. *J. Aircr.*, vol. 28, no. 1, Jan. 1991, pp. 22–28.

13. Chattopadhyay, Aditi; Walsh, Joanne L.; and Riley, Michael F.: Integrated Aerodynamic Load/ Dynamic Optimization of Helicopter Rotor Blades. *J. Aircr.*, vol. 28, no. 1, Jan. 1991, pp. 58–65.

14. Walsh, Joanne L.; LaMarsh, William J., II; and Adelman, Howard M.: *Fully Integrated Aerodynamic/Dynamic Optimization of Helicopter Rotor Blades.* NASA TM-104226, 1992.

15. Adelman, Howard M.; Walsh, Joanne L.; and Pritchard, Jocelyn I.: *Recent Advances in Multidisciplinary Optimization of Rotorcraft.* NASA TM-107665, AVSCOM TR-92-B-012, 1992.

16. Straub, F. K.; Callahan, C. B.; and Culp, J. D.: Rotor Design Optimization Using a Multidisciplinary Approach. AIAA-91-0477, Jan. 1991.

17. Callahan, Cynthia B.; and Straub, Friedrich K.: Design Optimization of Rotor Blades for Improved Performance and Vibration. *Proceedings of the 47th Annual Forum of the American Helicopter Society,* Volume 2, May 1991, pp. 869–882.

18. He, C. J.; and Peters, D. A.: Optimization of Rotor Blades for Combined Structural, Dynamic, and Aerodynamic Properties. *Struct. Optim.*, vol. 5, 1992, pp. 37–44.

19. Chattopadhyay, Aditi; and Narayan, Johnny R.: Optimum Design of High Speed Prop-Rotors Using a Multidisciplinary Approach. *Proceedings of the 48th Annual Forum of the American Helicopter Society,* Volume 2, June 1992, pp. 1167–1177.

20. Sobieszczanski-Sobieski, Jaroslaw: *Two Alternative Ways for Solving the Coordination Problem in Multilevel Optimization.* NASA TM-104036, 1991.

21. Chattopadhyay, Aditi; McCarthy, Thomas R.; and Pagaldipti, Narayanan: A Multilevel Decomposition Procedure for Efficient Design Optimization of Helicopter Rotor Blades. *Proceedings of the 19th European Rotorcraft Forum,* Sept. 1993, Paper No. G7.

22. Sobieszczanski-Sobieski, Jaroslaw; James, Benjamin B.; and Dovi, A. R.: Structural Optimization by Generalized, Multilevel Optimization. *AIAA J.*, vol. 23, no. 11, Nov. 1985, pp. 1775–1782.

23. Wrenn, Gregory A.; and Dovi, Augustine R.: Multilevel Decomposition Approach to the Preliminary Sizing of a Transport Aircraft Wing. *J. Aircr.*, vol. 25, July 1988, pp. 632–638.

24. Zeiler, Thomas A.; and Gilbert, Michael G.: Integrated Control/Structure Optimization by Multilevel Decomposition. *A Collection of Technical Papers—AIAA/ASME/ASCE/AHS/ASC 31st Structures, Structural Dynamics and Materials Conference,* Part 1, Apr. 1990, pp. 247–257.

25. Sobieszczanski-Sobieski, Jaroslaw: *A Linear Decomposition Method for Large Optimization Problems—Blueprint for Development.* NASA TM-83248, 1982.

26. Sobieszczanski-Sobieski, Jaroslaw; Barthelemy, Jean-Francois; and Riley, Kathleen M.: Sensitivity of Optimum Solutions to Problem Parameters. *AIAA J.*, vol. 20, no. 9, Sept. 1982, pp. 1291–1299.

27. Thareja, Rajiv; and Haftka, Raphael T.: Numerical Difficulties Associated With Using Equality Constraints To Achieve Multi-Level Decomposition in Structural Optimization. *A Collection of Technical Papers—AIAA/ASME/ASCE/AHS 27th Structures, Structural Dynamics*

and *Materials Conference*, Part 1, May 1986, pp. 21–28. (Available as AIAA-86-0854.)

28. Barthelemy, Jean-Francois M.; and Sobieszczanski-Sobieski, Jaroslaw: Optimum Sensitivity Derivatives of Objective Functions in Nonlinear Programming. *AIAA J.*, vol. 21, no. 6, June 1983, pp. 913–915.

29. Kreisselmeir, G.; and Steinhauser, R.: Systematic Control Design by Optimizing a Vector Performance Index. *Computer Aided Design on Control Systems*, W. A. Cuenod, ed., Pergamon Press, 1980, pp. 113–117.

30. Gessow, Alfred; and Myers, Garry C., Jr.: *Aerodynamics of the Helicopter.* MacMillan Co., 1952. (Republished 1967 by Frederick Ungar Publ. Co.)

31. Johnson, Wayne: *A Comprehensive Analytical Model of Rotorcraft Aerodynamics and Dynamics—Johnson Aeronautics Version. Volume II: User's Manual.* CAMRAD/JA, Johnson Aeronautics (Palo Alto, California), 1988.

32. Rosenstein, Harold; and Clark, Ross: Aerodynamic Development of the V-22 Tilt Rotor. *Proceedings of the 12th European Rotorcraft Forum*, Sept. 1986, Paper No. 14.

33. Vanderplaats, Garret N.: *CONMIN—A FORTRAN Program for Constrained Function Minimization, User's Manual.* NASA TM X-62282, 1973.

34. Walsh, Joanne Lynn: Computer-Aided Design of Light Aircraft to Meet Certain Aerodynamic and Structural Requirements. M. Eng. in Thermal Eng., Thesis, Old Dominion Univ., Aug. 1973.

35. Noonan, Kevin W.: *Aerodynamic Characteristics of Two Rotorcraft Airfoils Designed for Application to the Inboard Region of a Main Rotor Blade.* NASA TP-3009, AVSCOM TR-90-B-005, 1990.

36. Bingham, Gene J.; and Noonan, Kevin W.: *Two-Dimensional Aerodynamic Characteristics of Three Rotorcraft Airfoils at Mach Numbers From 0.35 to 0.90.* NASA TP-2000, AVRADCOM TR-82-B-2, 1982.

37. Wilbur, Matthew L.: Experimental Investigation of Helicopter Vibration Reduction Using Rotor Blade Aeroelastic Tailoring. *Proceedings of the 47th Annual Forum of the American Helicopter Society*, Volume 2, May 1991, pp. 969–982.

38. Bruhn, E. F.: *Analysis and Design of Airplane Structure, Revised.* Tri-State Offset Co., 1945.

Table 1. Bounds for Design Variables Used in Optimization Examples

Quantity	Design variables	
	Lower bound	Upper bound
Twist, deg	−20.0	−5.0
Taper initiation, r/R	0.26	0.985
Taper ratio	0.05	5.0
Root chord, ft	0.05	0.833
EI_{xx}, lb-ft^2	50.00	20 000 000.0
EI_{zz}, lb-ft^2	5.00	1000.0
GJ, lb-ft^2	5.00	1000.0
EA, lb	1000.00	200 000 000.0
m_i, slug/ft	0	0.50
$y_i, r/R$	0.24	0.95
t_i, ft	0.00008	0.01
a_i, ft^2	0	0.00004

Table 2. Parameters and Flight Conditions Used in Optimization Examples

(a) Parameters

Minimum autorotational inertia, AI_{min}, lb-ft^2 . . . . 23.69
Allowable drag coefficient, $c_{d,all}$ 0.12
Minimum tip chord, $c_{t,min}$, ft 0.083
Number of blades, N 4

Number of aerodynamic segments:
 HOVT 19
 CAMRAD/JA 18
Number of structural segments 50

Number of design variables:
 Upper level 22
 Lower level . . . . 18 (6 per location)
Power available, P_a, hp 20
Blade radius, R, ft 4.68
Maximum blade mass, W, lb 3.5
Factor of safety, l_f 2.0
Frequency increment, Δf, per rev 0.1
Allowable average strain, ε_a, ft/ft 0.05
$ITER_{max}$ 40
ρ_{max} 300
Allowable stress, σ_a, lb/ft^2 . . . . 8.352×10^6
Young's modulus, E, lb/ft^2 . . . . 15.26×10^8

(b) Flight conditions

Rotational velocity (in Freon with density of 0.006 slug/ft^3), Ω, rpm 639.5
Hover tip Mach number 0.628

C_L:
 Hover 0.00810
 Forward flight 0.00810
 Maneuver 0.00985

C_D:
 Forward flight . . . . −0.000811
 Maneuver . . . . −0.000596

Advance ratio:
 Forward flight 0.35
 Maneuver 0.30

Table 3. Example 1: Rectangular-Planform Starting Point With Matched Stiffnesses

(a) Initial and final values for blade planform, performance measures,
and dynamic measures

Quantity	Initial value	Final value
Hover power, hp	14.81	14.50
Forward flight power, hp	13.26	12.96
Maneuver power, hp	12.22	11.94
Hub shear, lb	2.1	1.1
Objective function	20.578	19.9107
Twist, deg	-9.0	-11.47
Taper initiation, r/R	0.7	0.7010
Taper ratio	1.0	1.664
Root chord, ft	0.3449	0.3770
m_1, slug/ft	0	0.00027607
m_2, slug/ft	0	0.0031988
m_3, slug/ft	0	0.0020144
$y_1, r/R$		0.4503
$y_2, r/R$		0.5830
$y_3, r/R$		0.4534
Cycles to converge		76

(b) Initial and final values for constrained frequencies

Frequency, per rev	Initial value	Final value
$f_{b,3}$	2.60	2.68
$f_{b,4}$	3.77	4.57
$f_{b,5}$	4.52	4.88
$f_{b,6}$	7.22	7.55
$f_{t,1}$	7.30	7.30
$f_{t,2}$	3.61	3.83

(c) Final values for lower level design variables and upper level stiffnesses

Variable	Radial location 1 (root)	Radial location 2 (point of taper initiation)	Radial location 3 (tip)
Final lower level design variables			
t_1, ft	0.002366	0.002427	0.0004517
t_2, ft	0.003261	0.009954	0.0003766
t_4, ft	0.003414	0.009954	0.0003766
a_1, ft^2	0.00003341	0.00003293	0.00001610
a_2, ft^2	0.00001615	0.00003084	0.00001192
a_3, ft^2	0.00003281	0.00003293	0.00001610
Final upper level stiffnesses			
EI_{xx}, lb-ft^2	2057.0	2974.1	153.73
EI_{zz}, lb-ft^2	122.21	140.03	8.6135
GJ, lb-ft^2	127.93	128.53	5.8743
EA, lb	797 370	1 647 300	212 230

Table 4. Example 2: Tapered-Planform Starting Point With Matched Stiffnesses

(a) Initial and final values for blade planform, performance measures,
and dynamic measures

Quantity	Initial value	Final value
Hover power, hp	14.85	14.74
Forward flight power, hp	13.38	13.02
Maneuver power, hp	11.93	11.84
Hub shear, lb	0.6	0.66
Objective function	19.876	19.9326
Twist, deg	−16.0	−10.85
Taper initiation, r/R	0.8	0.37
Taper ratio	3.0	1.636
Root chord, ft	0.45	0.4932
m_1, slug/ft	0	0.008961
m_2, slug/ft	0	0.01354
m_3, slug/ft	0	0.0246
$y_1, r/R$		0.24
$y_2, r/R$		0.6164
$y_3, r/R$		0.6215
Cycles to converge		93

(b) Initial and final values for constrained frequencies

Frequency, per rev	Initial value	Final value
$f_{b,3}$	2.93	2.86
$f_{b,4}$	5.64	5.33
$f_{b,5}$	6.22	6.68
$f_{b,6}$	10.25	9.16
$f_{t,1}$	7.30	7.30
$f_{t,2}$	6.45	6.12

Table 5. Example 3: Tapered-Planform Starting Point With Unmatched Stiffnesses

(a) Initial and final values for blade planform, performance measures,
and dynamic measures

Quantity	Initial value	Final value
Hover power, hp	14.85	16.64
Forward flight power, hp	13.27	17.46
Maneuver power, hp	11.89	14.89
Hub shear, lb	0.186	2.45
Objective function	20.005	24.624
Twist, deg	−16.0	−11.98
Taper initiation, r/R	0.8	0.8893
Taper ratio	3.0	1.3148
Root chord, ft	0.45	0.7364
m_1, slug/ft		0.008546
m_2, slug/ft		0.0077966
m_3, slug/ft		0.0090299
$y_1, r/R$		0.32257
$y_2, r/R$		0.43886
$y_3, r/R$		0.39256
Cycles to converge		92

(b) Initial and final values for constrained frequencies

Frequency, per rev	Initial value	Final value
$f_{b,3}$	2.87	2.90
$f_{b,4}$	5.54	5.87
$f_{b,5}$	8.62	8.10
$f_{b,6}$	9.65	10.50
$f_{t,1}$	7.30	7.30
$f_{t,2}$	5.48	5.12

Table 6. Effect of Coordination Parameter (ε) on Multilevel Optimization Procedure

Quantity	Initial value	Final value at ε of—		
		0.4	−0.2	−0.4
Hover power, hp	14.81	14.44	14.60	14.50
Forward flight power, hp . . .	13.26	12.77	13.11	12.96
Maneuver power, hp	12.22	11.75	11.96	11.94
Hub shear, lb	2.1	0.2072	1.85	1.1
Objective function	20.58	19.48	20.22	19.9107
Twist, deg	−9.0	−13.32	−11.12	−11.47
Taper initiation, r/R	0.7	0.7859	0.8246	0.7010
Taper ratio	1.0	3.155	1.410	1.664
Root chord, ft	0.3449	0.3651	0.3606	0.3770
m_1, slug/ft	0	0.02571	0.00135	0.0002761
m_2, slug/ft	0	0.00211	0.0000995	0.0031988
m_3, slug/ft	0	0.00099	0.0000727	0.0020144
$y_1, r/R$		0.4124	0.3115	0.4503
$y_2, r/R$		0.4154	0.3950	0.5830
$y_3, r/R$		0.4382	0.4292	0.4533
Cycles to converge		90	152	76

Table 7. Case 1: Comparison of Single-Level and Two-Level Optimization
Procedures for Rectangular Starting Design

| Quantity | Initial value | Final value for approach— | |
		Single level	Two levels
Hover power, hp	14.81	14.42	14.50
Forward flight power, hp . . .	13.26	12.87	12.96
Maneuver power, hp	12.22	11.83	11.94
Hub shear, lb	2.1	1.27	1.1
Objective function	20.578	19.5469	19.9107
Twist, deg	−9.0	−13.25	−11.47
Taper initiation, r/R	0.7	0.7131	0.7010
Taper ratio	1.0	2.21	1.664
Root chord, ft	0.3449	0.3813	0.3770
m_1, slug/ft	0	0.003065	0.00027607
m_2, slug/ft	0	0.04554	0.0031988
m_3, slug/ft	0	0.013545	0.0020144
$y_1, r/R$		0.3073	0.4503
$y_2, r/R$		0.5132	0.5830
$y_3, r/R$		0.5061	0.4534
Feasible design		Yes	Yes

Table 8. Case 2: Comparison of Single-Level and Two-Level Optimization
Procedures for Tapered Starting Design

| Quantity | Initial value | Final value for approach— | |
		Single level	Two levels
Hover power, hp	14.85	14.41	14.74
Forward flight power, hp . . .	13.38	12.67	13.02
Maneuver power, hp	11.93	11.68	11.84
Hub shear, lb	0.6	0.7137	0.66
Objective function	19.876	19.377	19.9326
Twist, deg	−16.0	−13.22	−10.85
Taper initiation, r/R	0.8	0.4934	0.37
Taper ratio	3.0	3.098	1.636
Root chord, ft	0.45	0.4899	0.4932
m_1, slug/ft	0	0.002305	0.008961
m_2, slug/ft	0	0.1636	0.01354
m_3, slug/ft	0	0.2922	0.0246
$y_1, r/R$		0.2420	0.24
$y_2, r/R$		0.2420	0.6164
$y_3, r/R$		0.3610	0.6215
Feasible design		No	Yes

Table 9. Case 3: Multilevel Approach Starting From Feasible
Single-Level Optimization Solution

Quantity	Initial value from single-level approach	Final value from two-level approach
Hover power, hp	14.42	14.44
Forward flight power, hp . . .	12.87	12.89
Maneuver power, hp	11.83	11.83
Hub shear, lb	1.27	1.13
Objective function	19.5469	19.814
Twist, deg	−13.25	−12.51
Taper initiation, r/R	0.7131	0.7450
Taper ratio	2.21	2.4041
Root chord, ft	0.3813	0.3834
m_1, slug/ft	.003065	0.001920
m_2, slug/ft	0.04554	0.08434
m_3, slug/ft	0.013545	0.01985
$y_1, r/R$	0.3073	0.3487
$y_2, r/R$	0.5132	0.4397
$y_3, r/R$	0.5061	0.4421
Feasible design	Yes	Yes

Table 10. Case 4: Multilevel Approach Starting From Infeasible
Single-Level Optimization Solution

Quantity	Initial value from single-level approach	Final value from two-level approach
Hover power, hp	14.41	14.83
Forward flight power, hp . . .	12.67	13.35
Maneuver power, hp	11.68	11.96
Hub shear, lb	0.7137	1.29
Objective function	19.377	20.328
Twist, deg	−13.22	−10.80
Taper initiation, r/R	0.4934	0.36
Taper ratio	3.098	2.164
Root chord, ft	0.4899	0.5926
m_1, slug/ft	0.002305	0.0009530
m_2, slug/ft	0.1636	0.04803
m_3, slug/ft	0.2922	0.1042
$y_1, r/R$	0.2420	0.2913
$y_2, r/R$	0.2420	0.3221
$y_3, r/R$	0.3610	0.4373
Feasible design	No	Yes
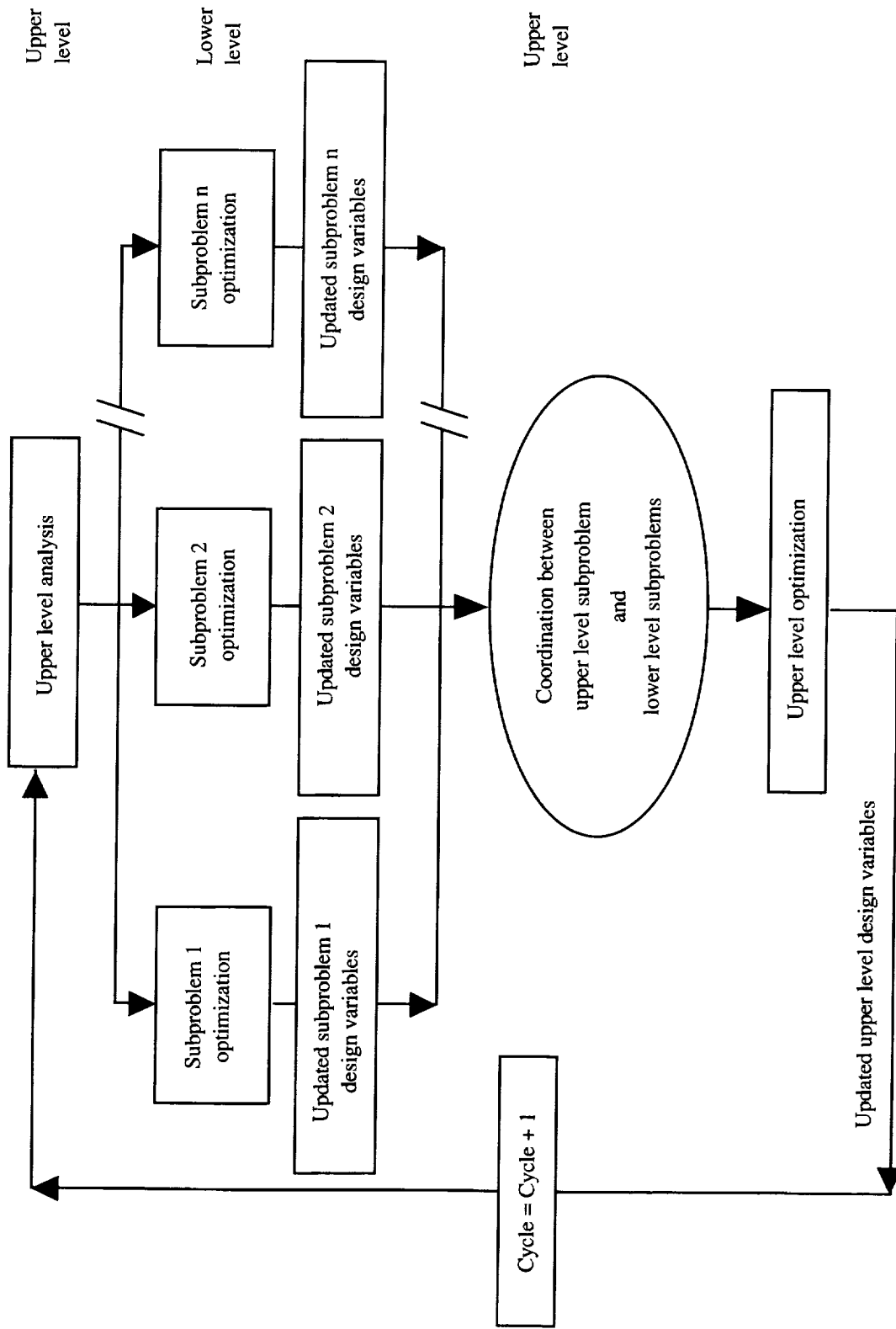
Figure 1. General multilevel optimization procedure with two levels.
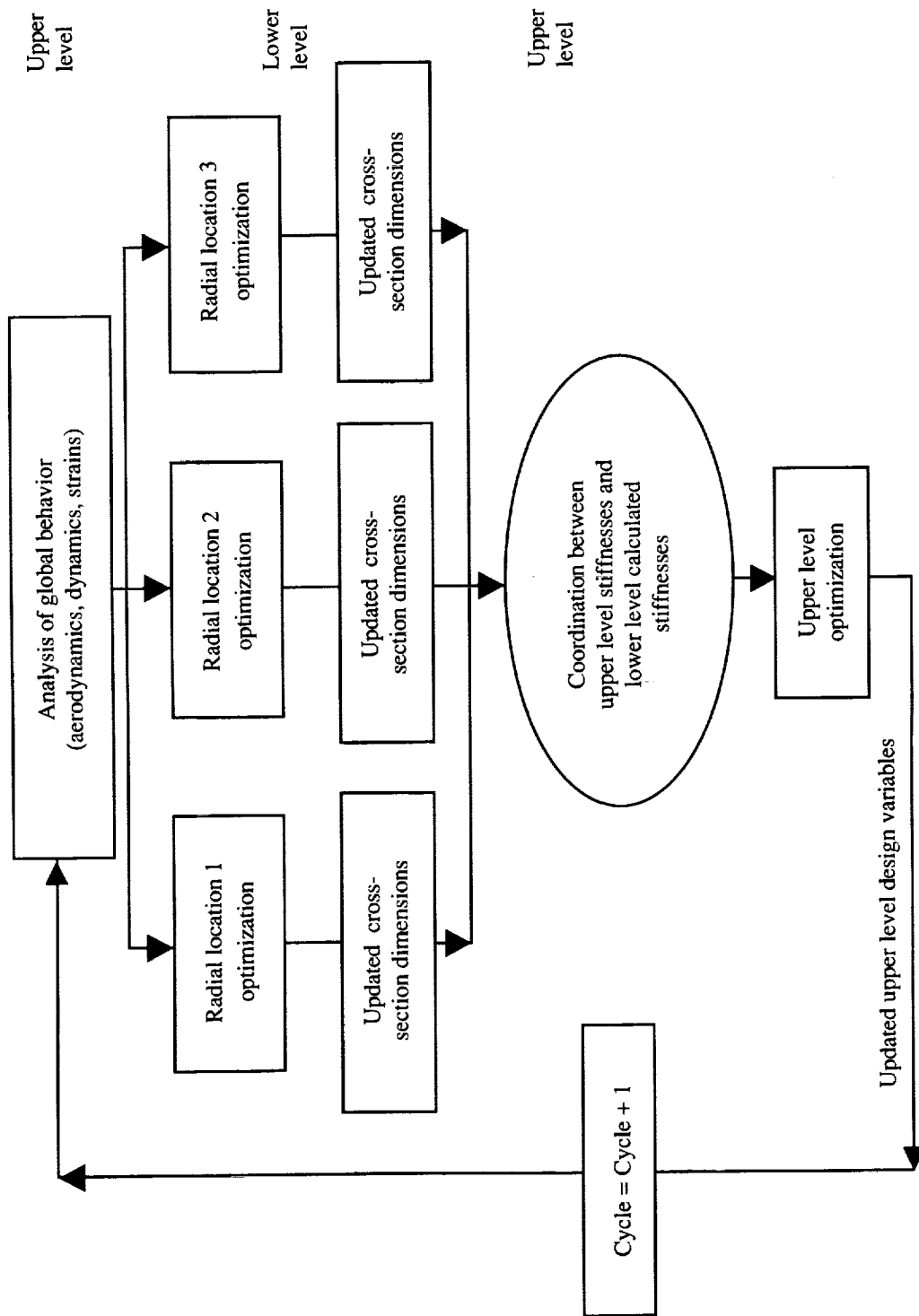
Figure 2. Multilevel strategy for rotor-blade aerodynamic, dynamic, and structural optimization.
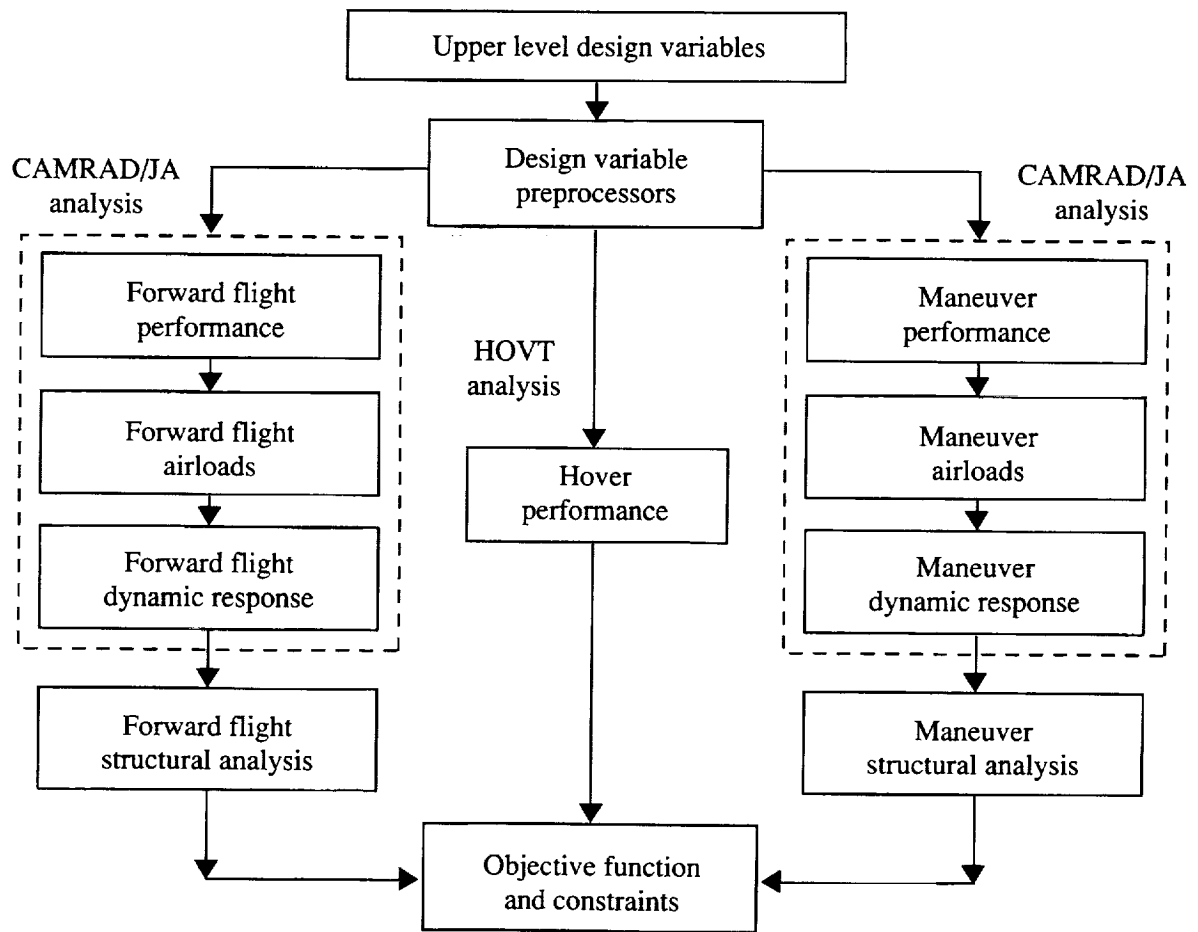
Figure 3. Flowchart of upper level analysis.

Point of taper initiation: $y_{tr} = r/R$
Root chord: c_r
Taper ratio: c_r/c_t
Maximum pretwist: θ_{tw}
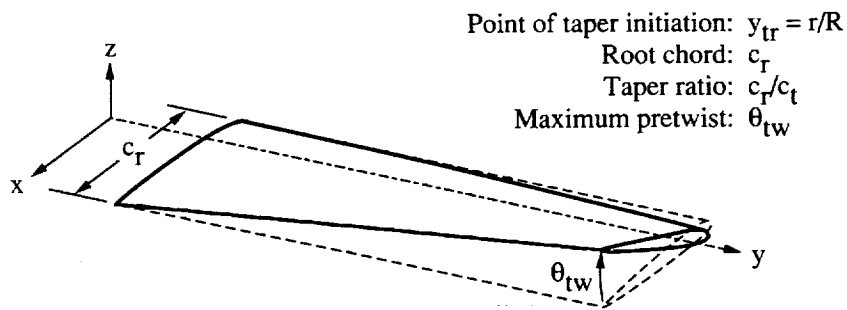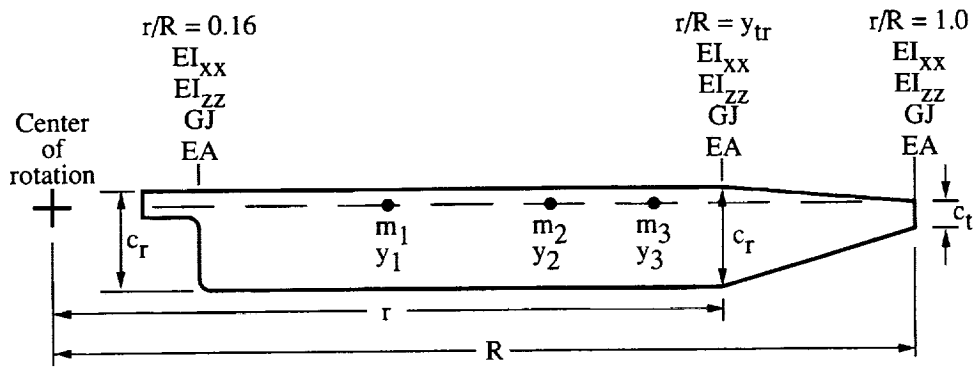
Figure 4. Upper level design variables.
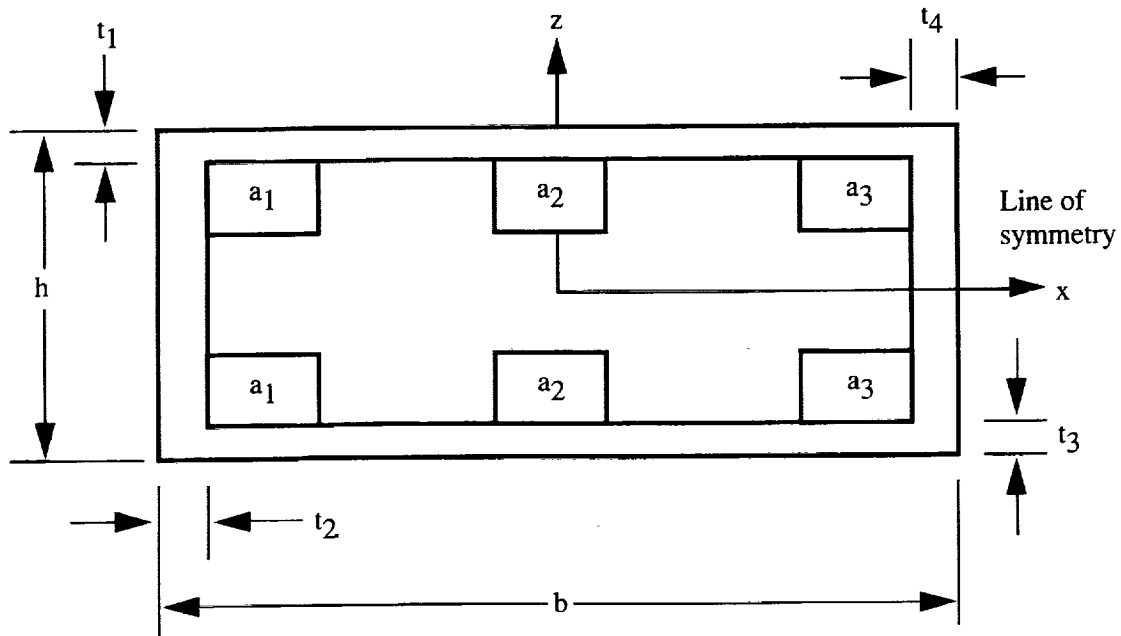
Figure 5. Lower level design variables.

34
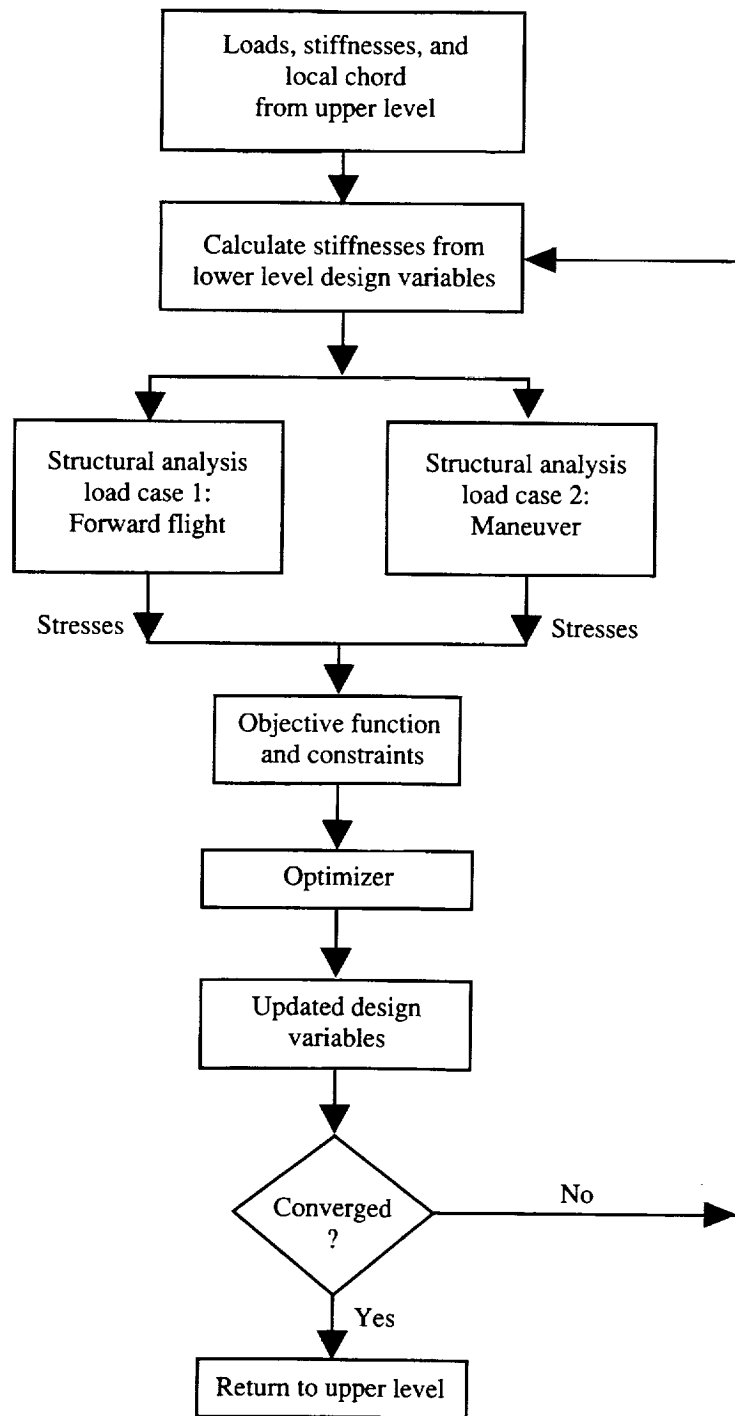
Figure 6. Lower level flowchart.
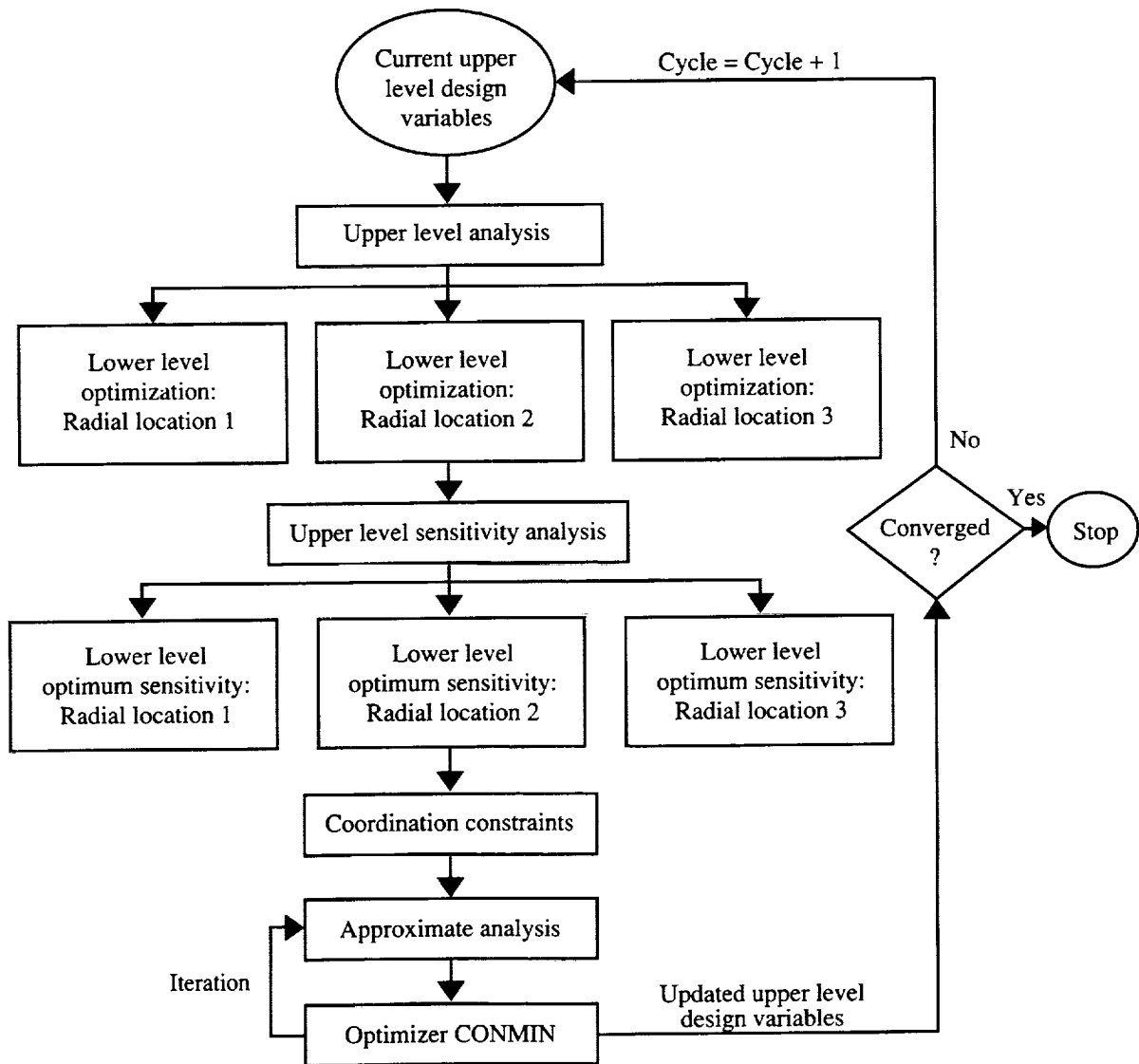
Figure 7. Overall optimization flowchart.

Center of
rotation

Twist = –9°
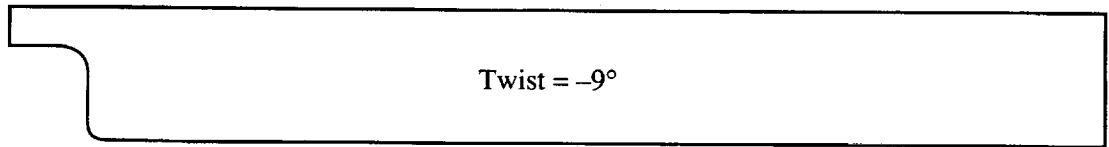
(a) Example 1: rectangular planform with matched upper and lower level stiffnesses.

Twist = –16°
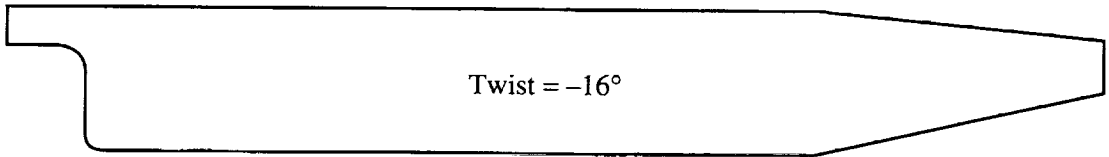
(b) Example 2: tapered planform with matched upper and lower level stiffnesses.

Twist = –16°
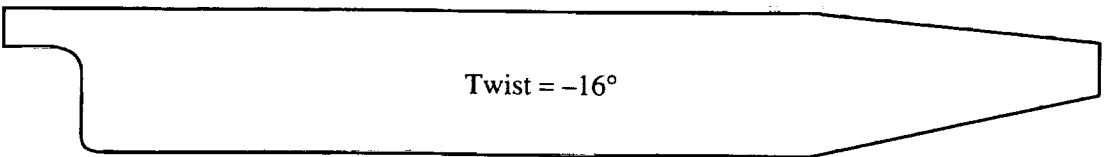
(c) Example 3: tapered planform with unmatched upper and lower level stiffnesses.
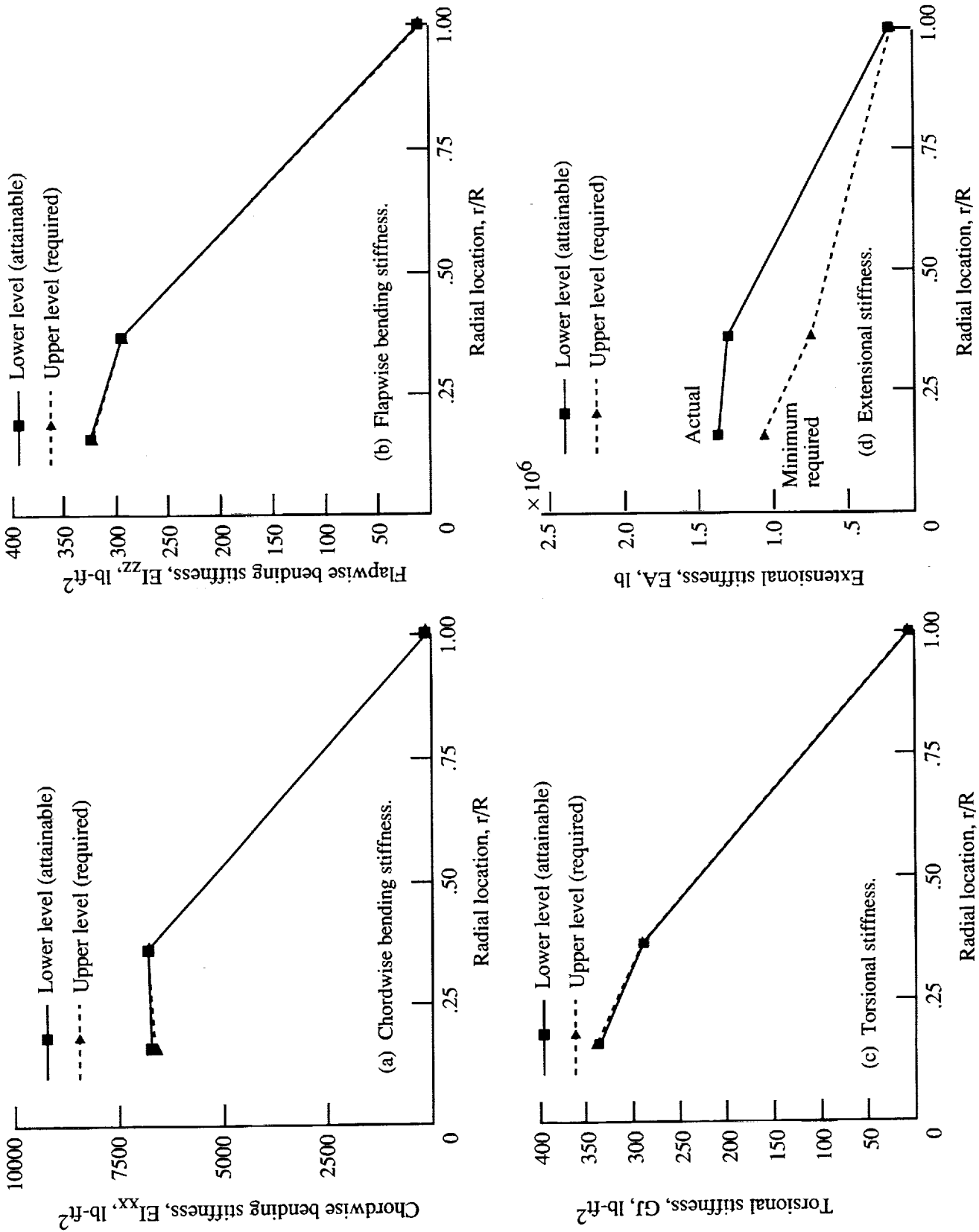
Figure 8. Starting points.
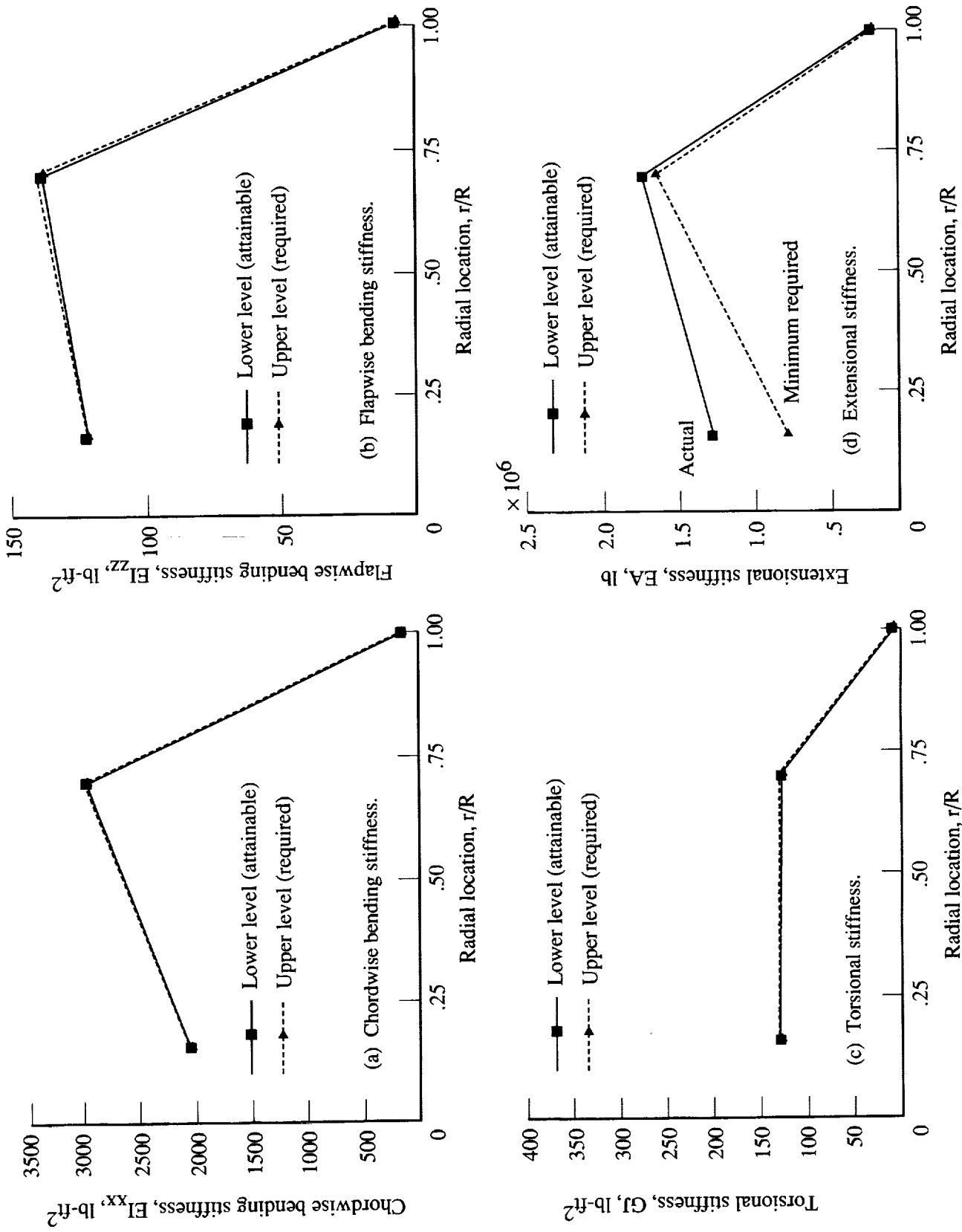
Figure 9. Final upper and lower level stiffness matching along blade radius for example 1.
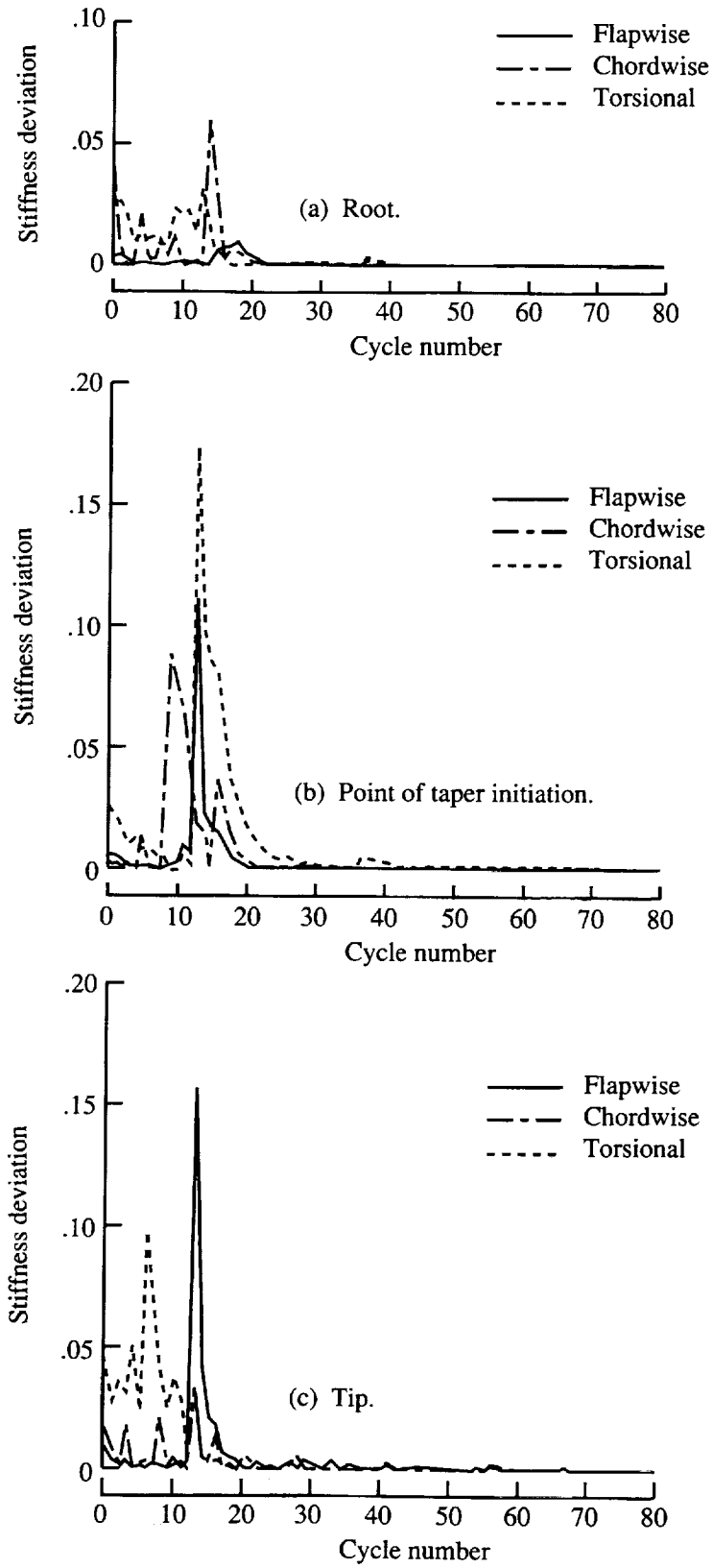
Figure 10. Convergence history of upper and lower level stiffness deviations for example 1.
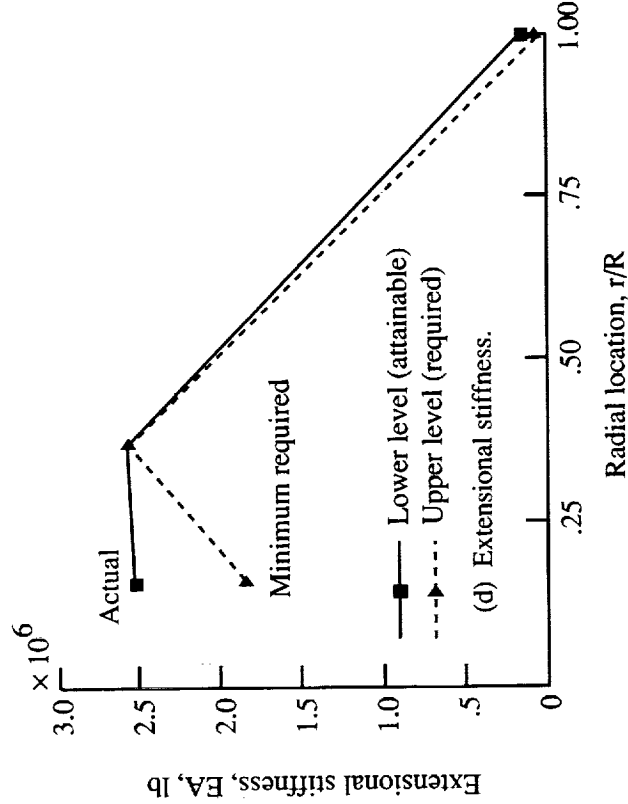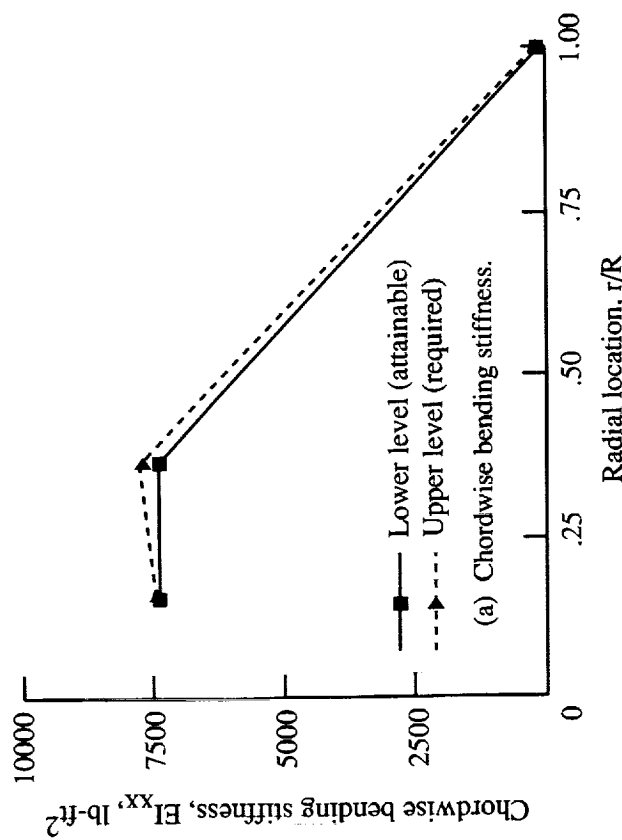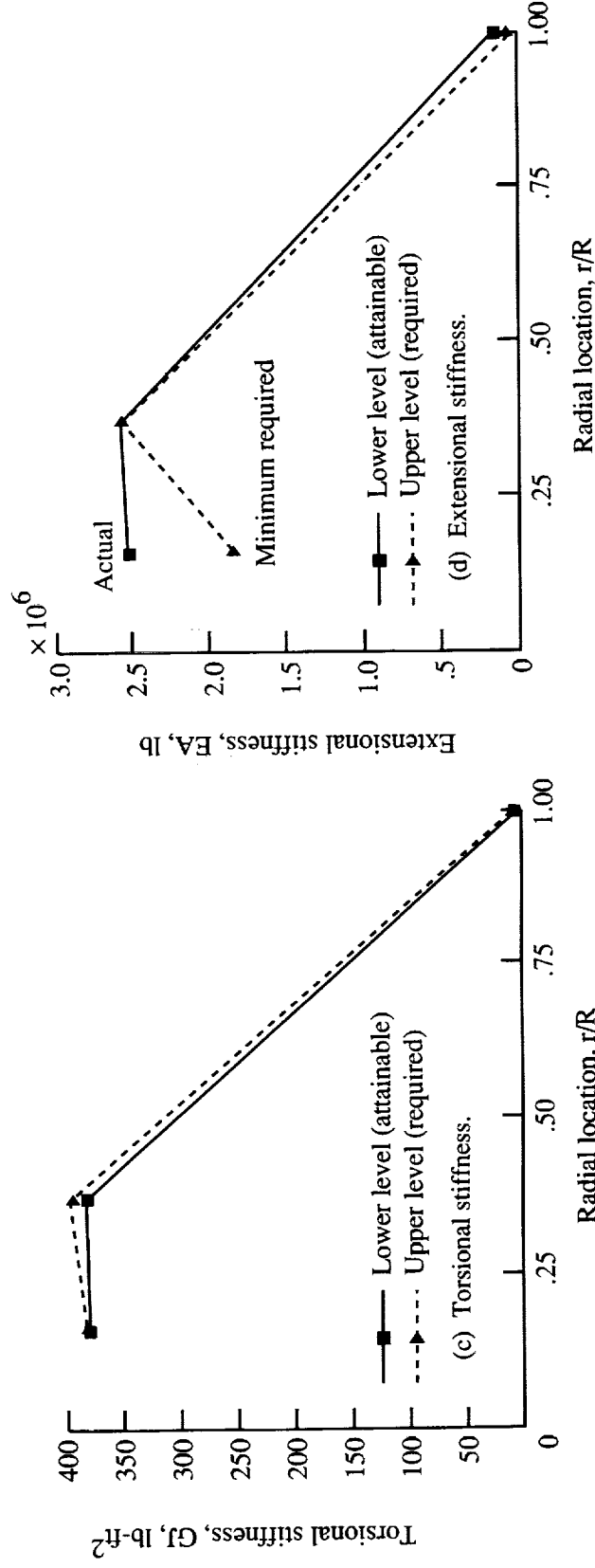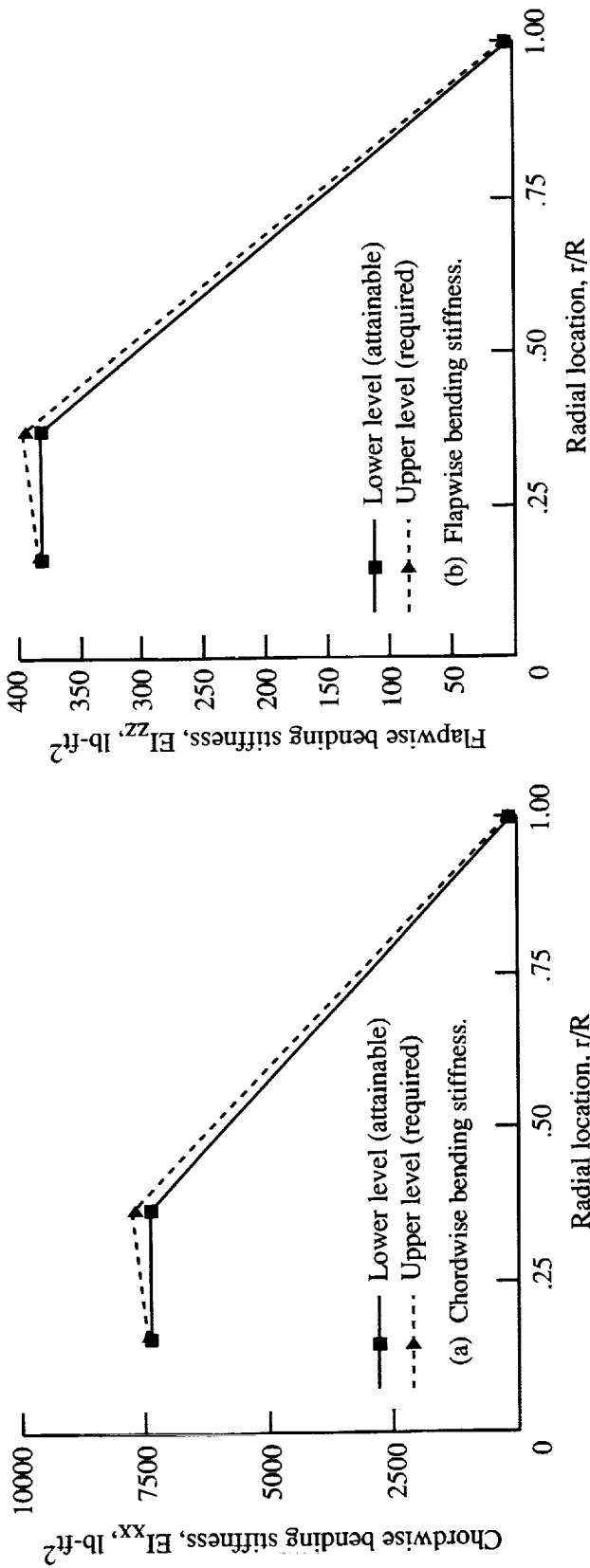
Figure 11. Final upper and lower level stiffness matching along blade radius for example 2.

40
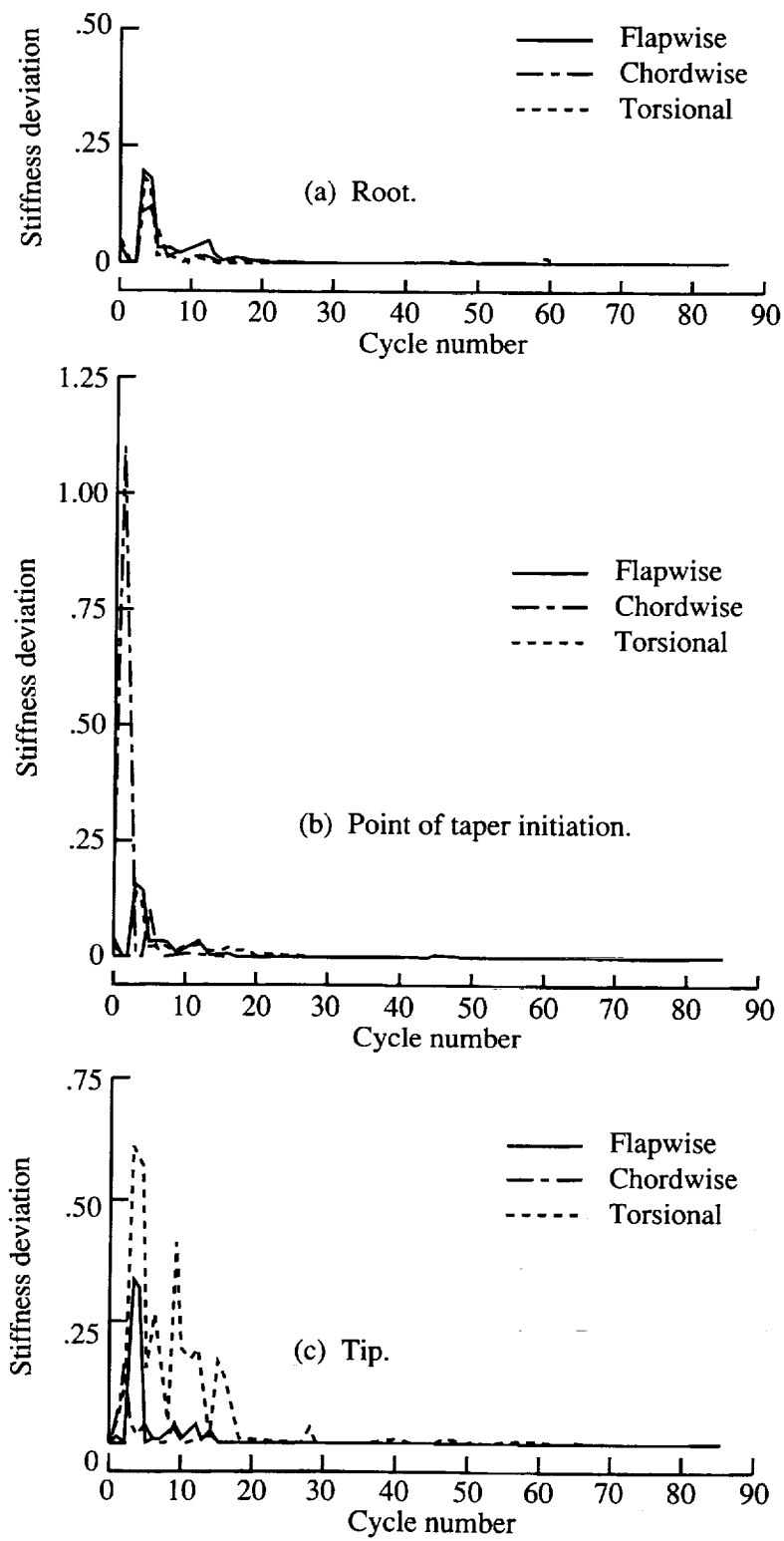
Figure 12. Convergence history of upper and lower level stiffness deviations for example 2.
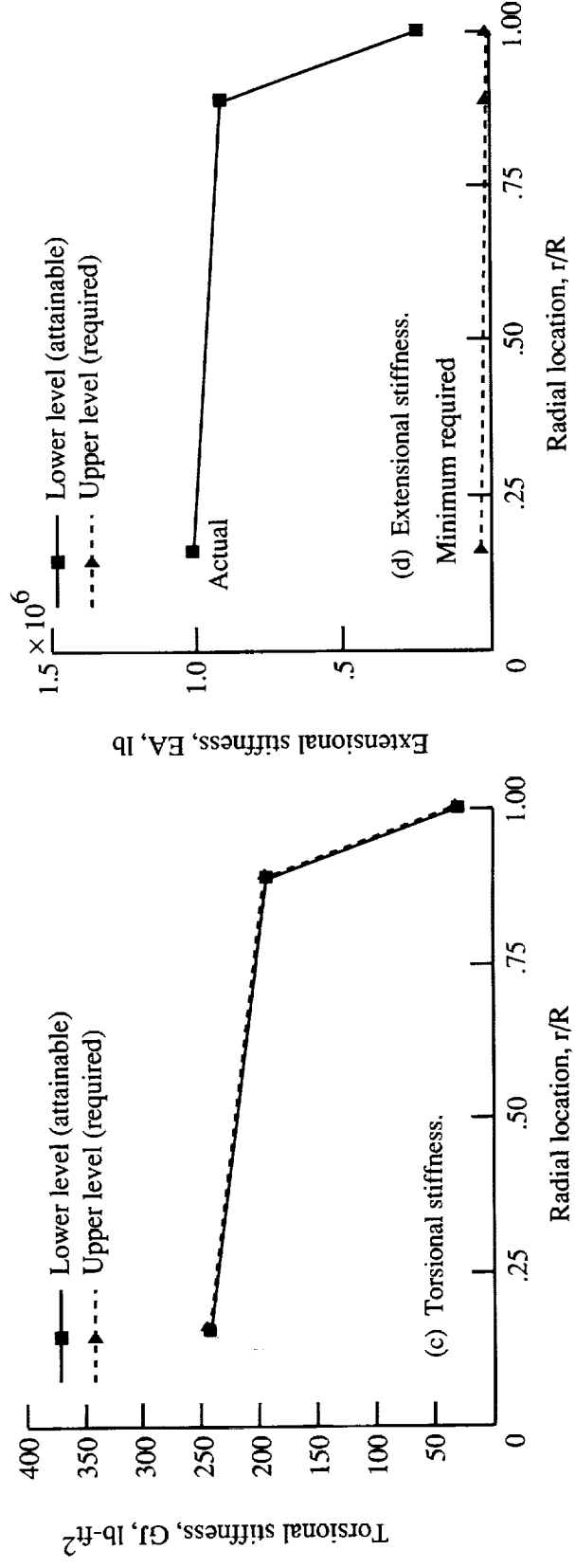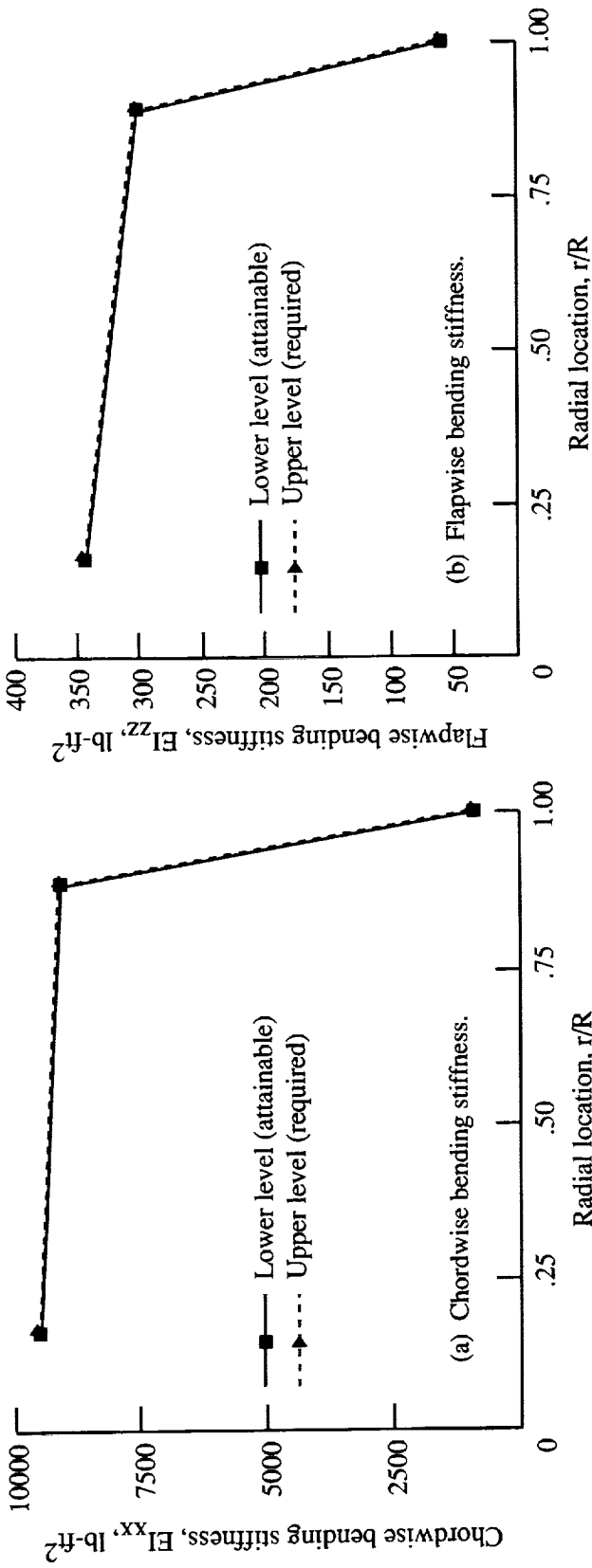
Figure 13. Final upper and lower level stiffness matching along blade radius for example 3.

42
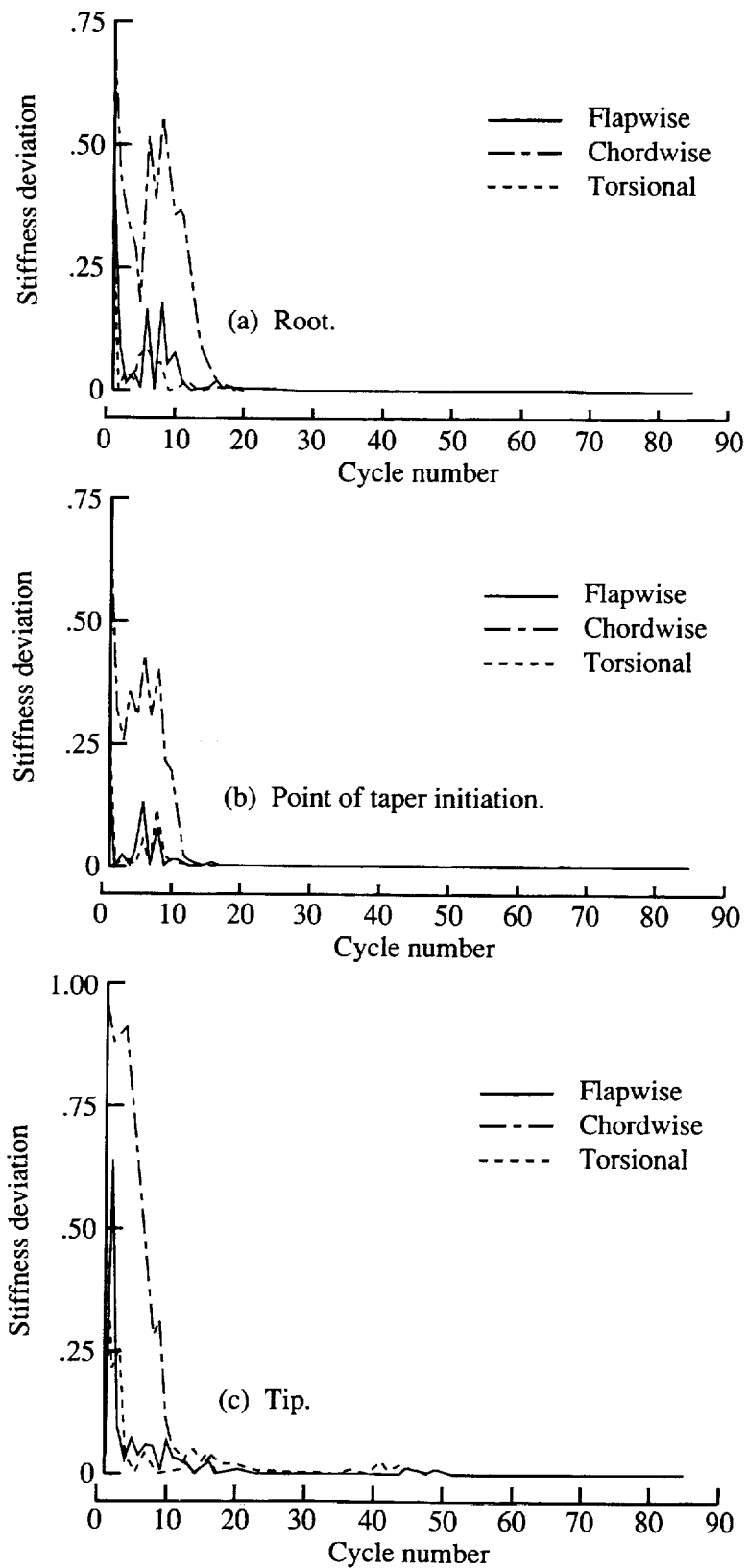
Figure 14. Convergence history of upper and lower level stiffness deviations for example 3.
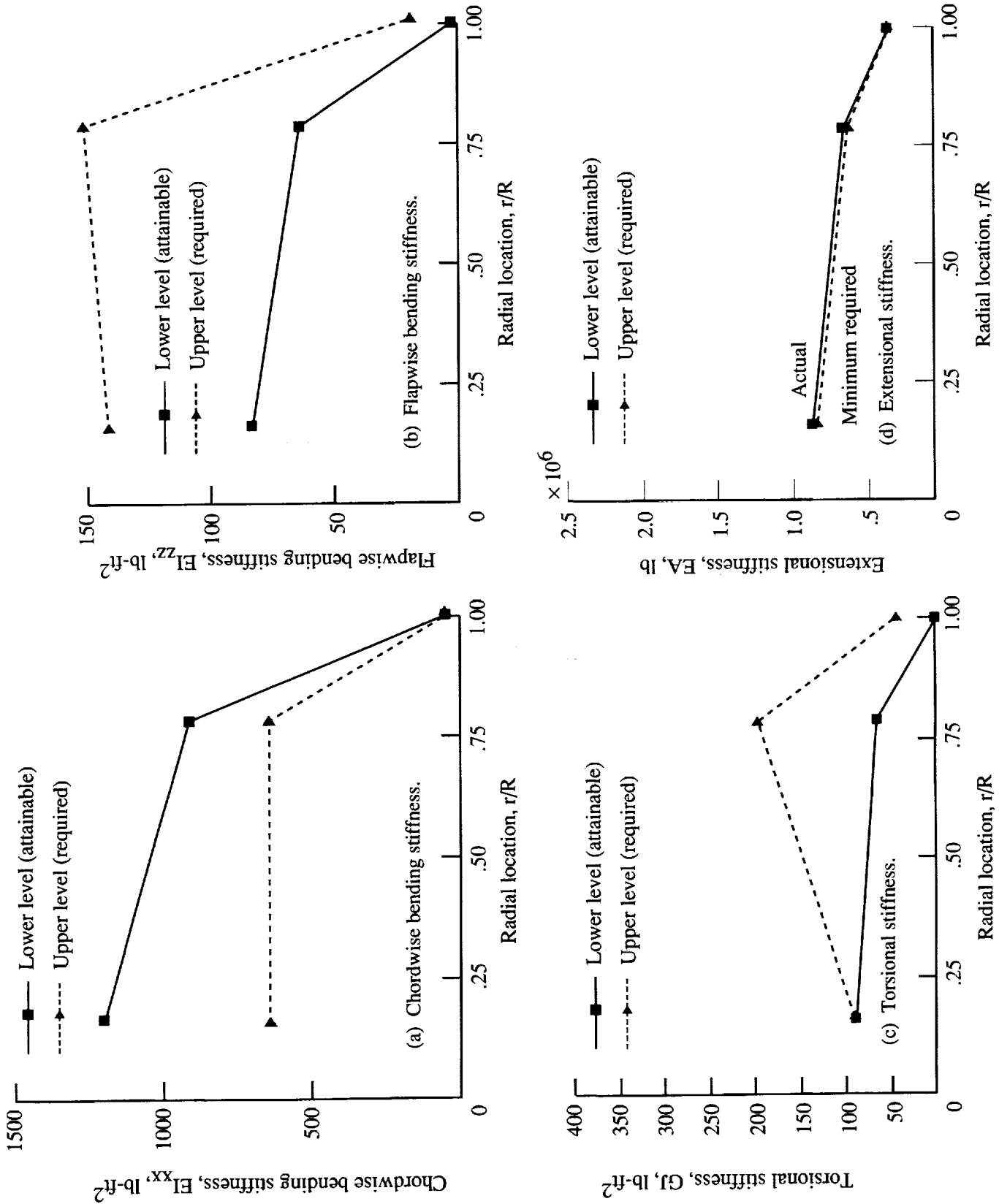
Figure 15. Final upper and lower level stiffness matching along blade radius for $\varepsilon = 0.4$.
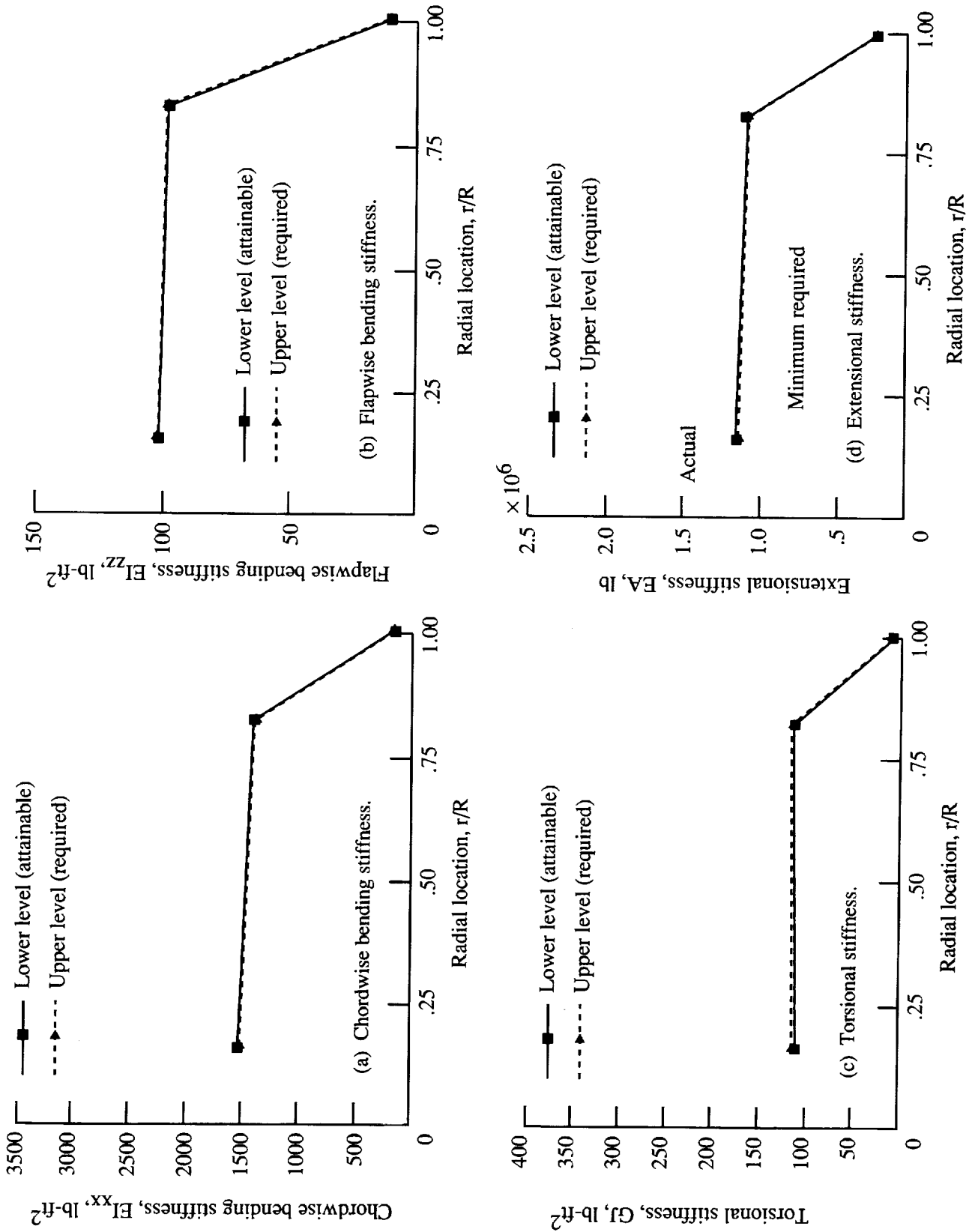
Figure 16. Final upper and lower level stiffness matching along blade radius for $\varepsilon = -0.2$.

(a) Chordwise bending stiffness.

(b) Flapwise bending stiffness.

(c) Torsional stiffness.

(d) Extensional stiffness.

Figure 17. Final upper and lower level stiffness matching along blade radius for case 4.

46
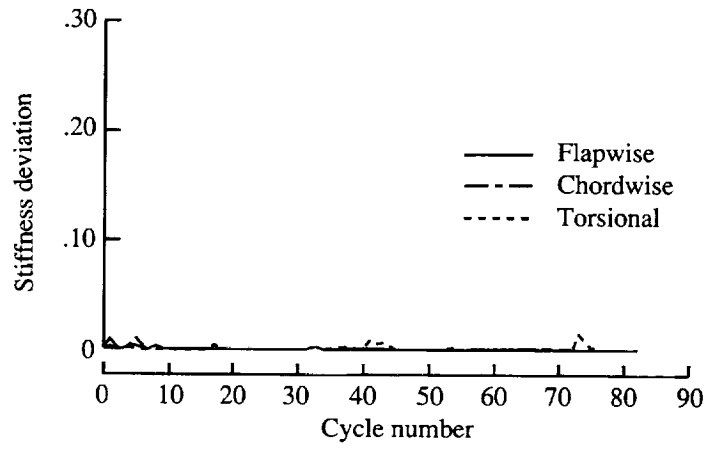
(a) Root.
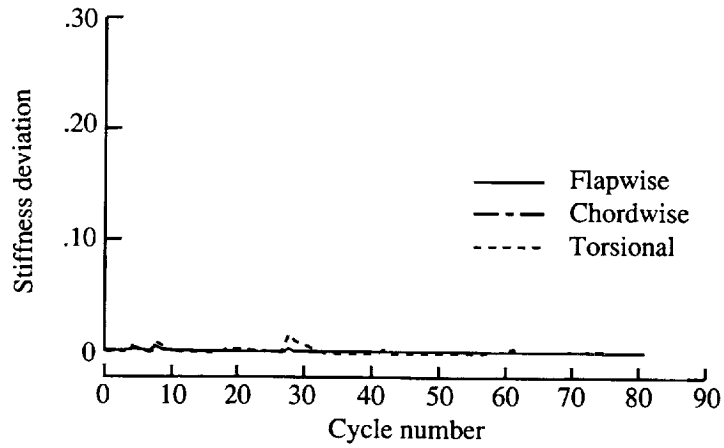
(b) Point of taper initiation.
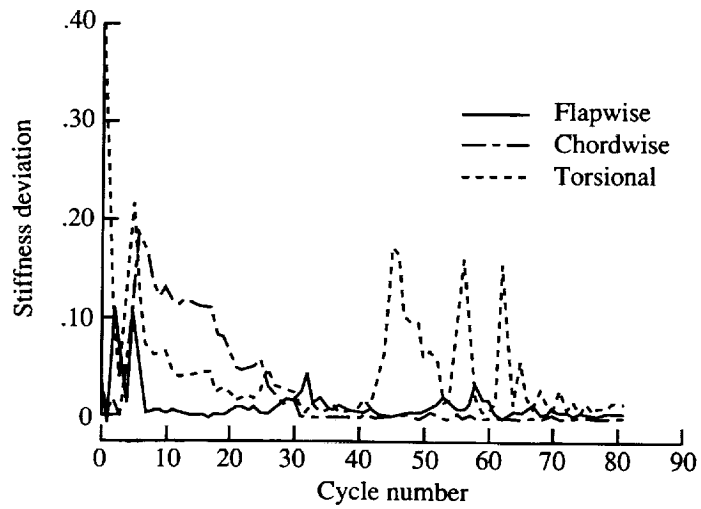
(c) Tip.

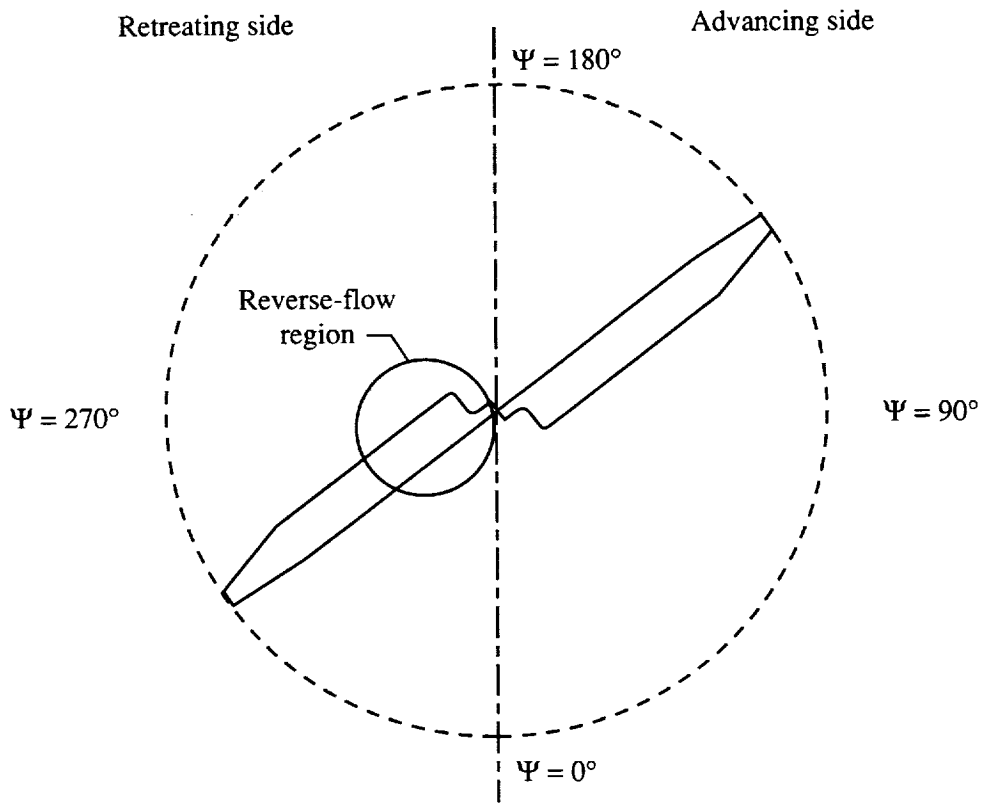Figure 18. Convergence history of upper and lower level stiffness deviations for case 4.
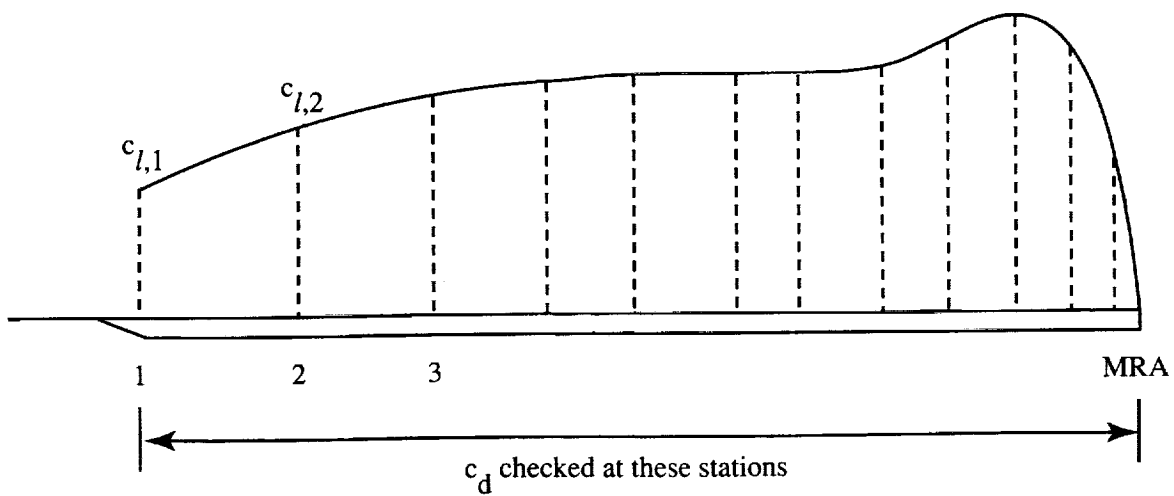
Figure 19. Rotor disk flow field.

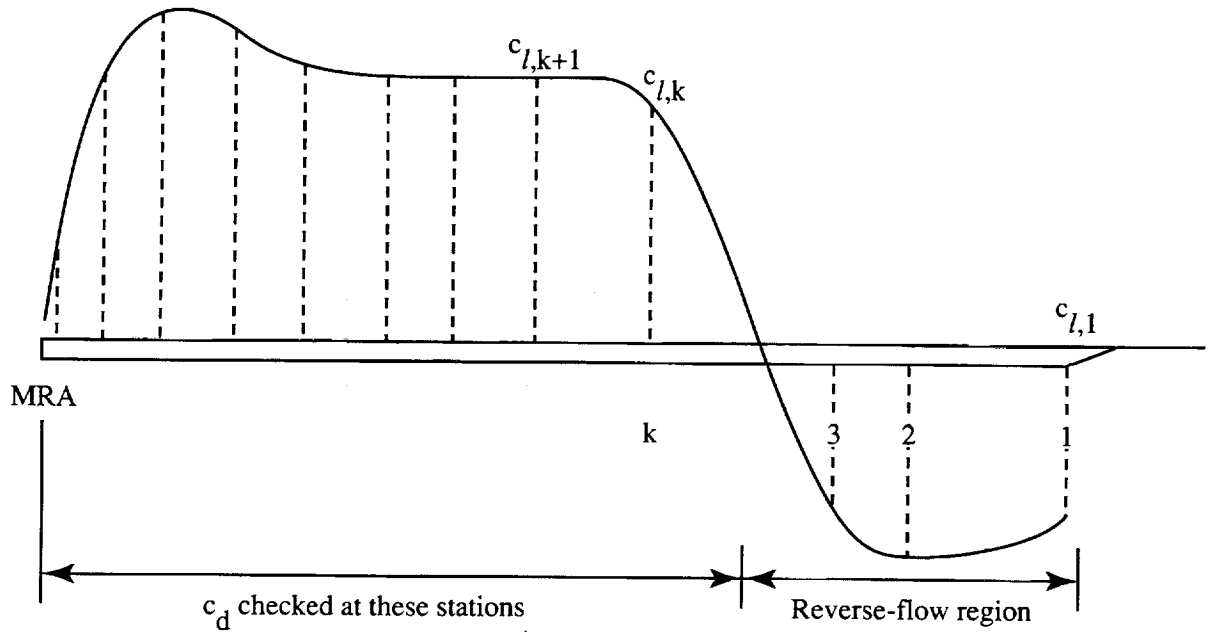Figure 20. Lift distribution on advancing side of rotor disk.

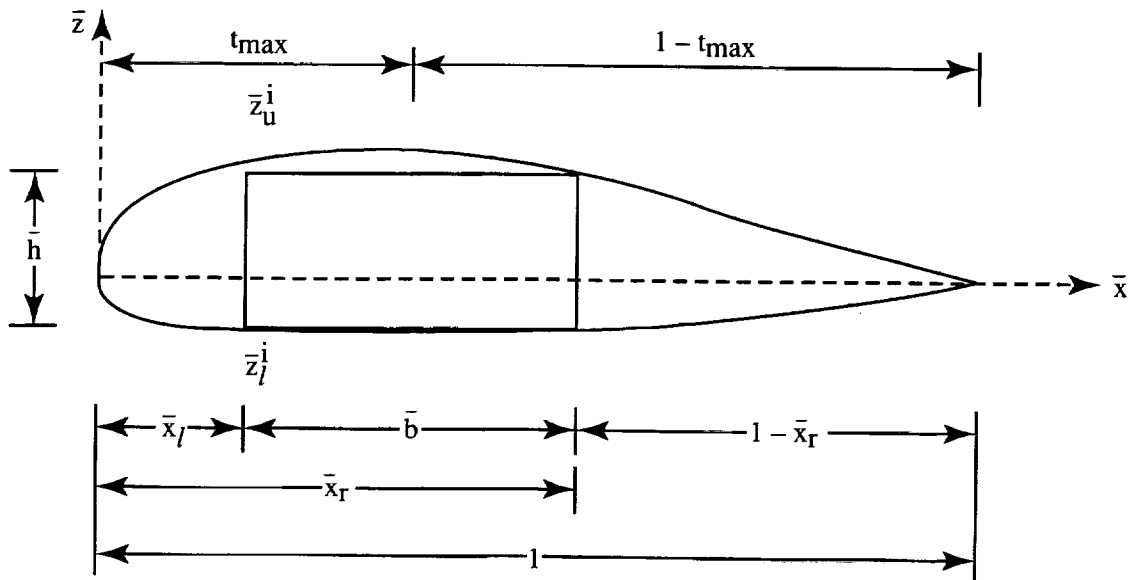Figure 21. Lift distribution on retreating side of rotor disk.

Figure 22. Wing box in RC(4)-10 airfoil.

REPORT DOCUMENTATION PAGE

Public reporting burden for this collection of information is estimated to average 1 hour per response, including the time for reviewing instructions, searching existing data sources, gathering and maintaining the data needed, and completing and reviewing the collection of information. Send comments regarding this burden estimate or any other aspect of this collection of information, including suggestions for reducing this burden, to Washington Headquarters Services, Directorate for Information Operations and Reports, 1215 Jefferson Davis Highway, Suite 1204, Arlington, VA 22202-4302, and to the Office of Management and Budget, Paperwork Reduction Project (0704-0188), Washington, DC 20503.

1. AGENCY USE ONLY *(Leave blank)*	2. REPORT DATE January 1995	3. REPORT TYPE AND DATES COVERED Technical Paper	

4. TITLE AND SUBTITLE
Integrated Aerodynamic/Dynamic/Structural Optimization of
Helicopter Rotor Blades Using Multilevel Decomposition

5. FUNDING NUMBERS

WU 505-63-36-06

PR 1L16241A47AB

6. AUTHOR(S)
Joanne L. Walsh, Katherine C. Young, Jocelyn I. Pritchard,
Howard M. Adelman, and Wayne R. Mantay

7. PERFORMING ORGANIZATION NAME(S) AND ADDRESS(ES)
NASA Langley Research Center   Vehicle Structures Directorate
Hampton, VA 23681-0001   U.S. Army Research Laboratory
                               NASA Langley Research Center
                               Hampton, VA 23681-0001

8. PERFORMING ORGANIZATION REPORT NUMBER

L-17233

9. SPONSORING/MONITORING AGENCY NAME(S) AND ADDRESS(ES)
National Aeronautics and Space Administration
Washington, DC 20546-0001
           and
U.S. Army Research Laboratory
Adelphi, MD 20783-1145

10. SPONSORING/MONITORING AGENCY REPORT NUMBER
NASA TP-3465

ARL-TR-518

11. SUPPLEMENTARY NOTES
Walsh, Young, and Adelman: Langley Research Center, Hampton, VA; Pritchard: Vehicle Structures Directorate, ARL, Langley Research Center, Hampton, VA; Mantay: JRPO, Aeroflightdynamics Directorate, ATCOM, Langley Research Center, Hampton, VA.

12a. DISTRIBUTION/AVAILABILITY STATEMENT

Unclassified–Unlimited
Subject Category 05
Availability: NASA CASI (301) 621-0390

12b. DISTRIBUTION CODE

13. ABSTRACT *(Maximum 200 words)*
This paper describes an integrated aerodynamic/dynamic/structural (IADS) optimization procedure for helicopter rotor blades. The procedure combines performance, dynamics, and structural analyses with a general-purpose optimizer using multilevel decomposition techniques. At the upper level, the structure is defined in terms of global quantities (stiffnesses, mass, and average strains). At the lower level, the structure is defined in terms of local quantities (detailed dimensions of the blade structure and stresses). The IADS procedure provides an optimization technique that is compatible with industrial design practices in which the aerodynamic and dynamic designs are performed at a global level and the structural design in carried out at a detailed level with considerable dialogue and compromise among the aerodynamic, dynamic, and structural groups. The IADS procedure is demonstrated for several examples.

14. SUBJECT TERMS
Rotor blades; Helicopters; Optimization; Multidisciplinary design

15. NUMBER OF PAGES
50

16. PRICE CODE
A04

17. SECURITY CLASSIFICATION OF REPORT Unclassified	18. SECURITY CLASSIFICATION OF THIS PAGE Unclassified	19. SECURITY CLASSIFICATION OF ABSTRACT Unclassified	20. LIMITATION OF ABSTRACT

NSN 7540-01-280-5500